Article

Neuron

# A VTA GABAergic Neural Circuit Mediates Visually Evoked Innate Defensive Responses

## Graphical Abstract

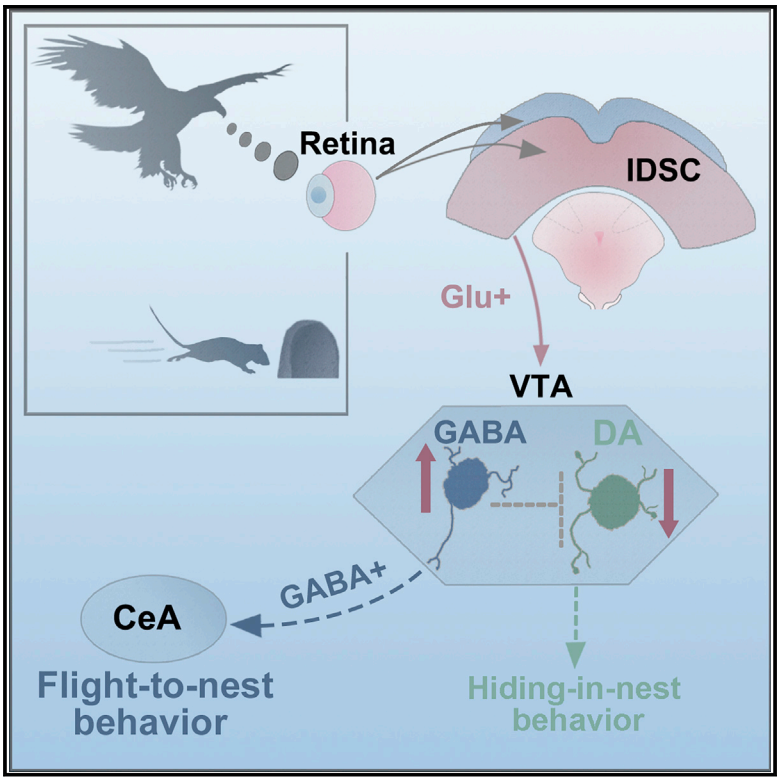


## Authors

Zheng Zhou, Xuemei Liu, Shanping Chen, ..., Guoping Feng, Fuqiang Xu, Liping Wang

## Correspondence

fuqiang.xu@wipm.ac.cn (F.X.), lp.wang@siat.ac.cn (L.W.)

## In Brief

Zhou et al. identified a neural circuit related to VTA$^{GABA+}$ neurons that mediates visually evoked innate defensive responses, involving the SC$^{Glut+}$- VTA$^{GABA+}$-CeA pathway.

## Highlights

- VTA$^{GABA+}$ neurons mediate looming-evoked innate defensive responses
- SC activates VTA$^{GABA+}$ neurons and mediates innate defensive behaviors
- CeA is a downstream target of the SC-VTA$^{GABA+}$ pathway
- CeA-projecting VTA$^{GABA+}$ involved in looming-evoked defensive behaviors

Zhou et al., 2019, Neuron *103*, 473–488
August 7, 2019 
https://doi.org/10.1016/j.neuron.2019.05.027

CellPress

Neuron
Article

# A VTA GABAergic Neural Circuit Mediates Visually Evoked Innate Defensive Responses

Zheng Zhou,[1,2,6] Xuemei Liu,[1,2,6] Shanping Chen,[1,2] Zhijian Zhang,[3] Yuanming Liu,[1] Quentin Montardy,[1] Yongqiang Tang,[1,2] Pengfei Wei,[1] Nan Liu,[1,2] Lei Li,[1] Ru Song,[1] Juan Lai,[1] Xiaobin He,[3] Chen Chen,[1] Guoqiang Bi,[4] Guoping Feng,[5] Fuqiang Xu,[3,7,*] and Liping Wang[1,2,7,*]

[1]Shenzhen Key Lab of Neuropsychiatric Modulation and Collaborative Innovation Center for Brain Science, Guangdong Provincial Key Laboratory of Brain Connectome and Behavior, CAS Center for Excellence in Brain Science and Intelligence Technology, Brain Cognition and Brain Disease Institute (BCBDI), Shenzhen Institutes of Advanced Technology, Chinese Academy of Sciences, Shenzhen-Hong Kong Institute of Brain Science-Shenzhen Fundamental Research Institutions, Shenzhen 518055, China

[2]University of the Chinese Academy of Sciences, Beijing 100049, China

[3]Center for Brain Science, Key Laboratory of Magnetic Resonance in Biological Systems and State Key Laboratory of Magnetic Resonance and Atomic and Molecular Physics, Wuhan Institute of Physics and Mathematics, CAS, Center for Excellence in Brain Science and Intelligence Technology, Chinese Academy of Sciences, Wuhan 430071, China

[4]School of Life Sciences, University of Science and Technology of China, Hefei, China

[5]McGovern Institute for Brain Research, Department of Brain and Cognitive Sciences, Massachusetts Institute of Technology, Cambridge, MA 02139, USA

[6]These authors contributed equally

[7]Lead Contact

*Correspondence: fuqiang.xu@wipm.ac.cn (F.X.), lp.wang@siat.ac.cn (L.W.)

https://doi.org/10.1016/j.neuron.2019.05.027

## SUMMARY

**Innate defensive responses are essential for animal survival and are conserved across species. The ventral tegmental area (VTA) plays important roles in learned appetitive and aversive behaviors, but whether it plays a role in mediating or modulating innate defensive responses is currently unknown. We report that VTA$^{GABA+}$ neurons respond to a looming stimulus. Inhibition of VTA$^{GABA+}$ neurons reduced looming-evoked defensive flight behavior, and photoactivation of these neurons resulted in defense-like flight behavior. Using viral tracing and electrophysiological recordings, we show that VTA$^{GABA+}$ neurons receive direct excitatory inputs from the superior colliculus (SC). Furthermore, we show that glutamatergic SC-VTA projections synapse onto VTA$^{GABA+}$ neurons that project to the central nucleus of the amygdala (CeA) and that the CeA is involved in mediating the defensive behavior. Our findings demonstrate that aerial threat-related visual information is relayed to VTA$^{GABA+}$ neurons mediating innate behavioral responses, suggesting a more general role of the VTA.**

## INTRODUCTION

The ventral tegmental area (VTA) is a heterogeneous nucleus including dopaminergic (DA+), Gamma-aminobutyric acid (GABA)ergic (GABA+), and glutamatergic (Glut+) neurons (Dobi et al., 2010; Morales and Margolis, 2017; Yamaguchi et al., 2007), and its dysfunction has been implicated in depression (Nestler and Carlezon, 2006), schizophrenia (Davis et al., 1991), and addiction (Lüscher and Malenka, 2011). Dopamine neurons in the VTA have been extensively studied for their role in reward and aversive processing (Bromberg-Martin et al., 2010; Fields et al., 2007; Schultz, 1998). It is widely accepted that VTA$^{GABA+}$ neurons play an essential role in promoting aversion through inhibition of VTA$^{DA+}$ neurons (Bocklisch et al., 2013; Jennings et al., 2013a; Tan et al., 2012; van Zessen et al., 2012).

Recently, there has been an increase in evidence that demonstrates the role of GABA neurons in defensive processes, such as the involvement of GABA neurons in the acquisition of conditioned fear (Ciocchi et al., 2010; Haubensak et al., 2010) and predator-odor-evoked innate fear (Yang et al., 2016). In addition, it has been reported recently that dorsal raphe nucleus (DRN) GABA+ neurons are activated following looming stimulation (Huang et al., 2017), that zona incerta (ZI) GABA+ neuronal projections to the periaqueductal gray (PAG) drive innate defensive responses (Chou et al., 2018), and also that VTA$^{GABA+}$ neuronal projections to nucleus accumbens (NAc) enhance associative aversive learning (Brown et al., 2012).

In fact, the VTA also contributes to aversive cue processing, such as air puffs, foot shocks, and free fall (Brischoux et al., 2009; Matsumoto and Hikosaka, 2009; Mirenowicz and Schultz, 1996; Tan et al., 2012). Consistent with these findings, VTA$^{GABA+}$ neurons are evoked by foot shock stimulation, which induces conditioned place aversion (Tan et al., 2012). More importantly, it is of fundamental importance for animals across species to detect visual predator-like environmental stimuli and generate avoidance behavior when necessary. Environmental stimuli require multiple sensory modality inputs that enable the animal to avoid potential threats (LeDoux, 2012).

The VTA, which receives widespread inputs, not only encodes value signals but also encodes salience signals (Bromberg-Martin et al., 2010; Beier et al., 2015; Lammel et al., 2012; Morales

and Margolis, 2017; Watabe-Uchida et al., 2012). The superior colliculus (SC), a retinal recipient structure, is a vital source for conveying visual signals to VTA neurons, implicated in detecting biologically salient stimuli (Comoli et al., 2003; Dommett et al., 2005; Redgrave and Gurney, 2006). These findings hint that visual threatening signals, such as those derived from predator-like looming stimuli, may reach the VTA via the SC and that this pathway might play a role in processing of the innate defensive responses. Given this, we speculate that the VTA is involved in processing visual, potentially life-threatening signals, and if so, what the underlying cell-specific neural circuitry mechanisms are.

Selection and rapid execution of appropriate defensive responses, ranging from risk assessment, fighting, and freezing to flight and attack, can be essential for survival when an animal faces imminent danger (Tovote et al., 2016; Ydenberg and Dill, 1986). A laboratory-based experimental paradigm has been established, where an animal is exposed to an expanding dark disc (looming) stimulus to the upper visual field that mimics an approaching aerial predator (Yilmaz and Meister, 2013). This looming stimulus leads to innate defensive behaviors (e.g., flight-to-nest and hiding behaviors) (Yilmaz and Meister, 2013). This paradigm offers the opportunity to examine the neural circuitry underlying visually evoked innate defensive behaviors (Evans et al., 2018; Huang et al., 2017; Li et al., 2018; Salay et al., 2018; Shang et al., 2018; Wei et al., 2015; Zelikowsky et al., 2018; Zhao et al., 2014).

Using this looming-evoked flight-to-nest behavioral paradigm with mice, we found that VTA$^{GABA+}$ neurons were activated by aversive visual stimuli. Selective optogenetic inhibition and activation of VTA$^{GABA+}$ neurons showed that they were crucial for normal defense-like behavior. Tracing and electrophysiological data show that VTA$^{GABA+}$ neurons received glutamatergic inputs from the SC and sent long projections to the central nucleus of the amygdala (CeA), which were also likely involved in the defensive behavior. To the best of our knowledge, this is the first evidence showing the involvement of VTA$^{GABA+}$ neurons in innate, evolutionally conserved, visually evoked defensive responses.

## RESULTS

### VTA$^{GABA+}$ Neurons Respond to a Looming Stimulus, which Evokes Defensive Behaviors

According to previous work (Yilmaz and Meister, 2013), mice were placed in an open field with a nest as a hiding place, and presentation of an upper-field expanding dark disc stimulus (looming stimulus) mimicking the approach of an aerial predator triggered transient intermittent immobility followed by flight-to-nest and hiding-in-nest behavior (Figure 1A). We tested various looming stimuli, including a front-field expanding dark disc stimulus, an upper-field expanding white disc stimulus, a lower-field expanding dark disc stimulus, and an upper-field expanding dark disc stimulus, and found that only the upper-field expanding dark disc stimulus reliably triggered transient intermittent immobility followed by robust flight-to-nest and hiding-in-nest behavior (upper-field expanding dark disc stimulus evoked 1.83 ± 0.21 s latency of onset of flight; 3.07 ± 0.33 s to return to nest; hiding time < 1 min after onset of looming stimulus, 71.86% ± 6.83% time in nest; Figure S3E). Therefore, in the following experiments, we used this type of looming stimulus and henceforth refer to it as "looming" or "LS."

We found that looming led to higher VTA c-Fos expression compared with a lower-field LS control (Figure 1B). The distribution of c-Fos expression was located in the parabrachial and paranigral portion of the VTA. Tyrosine hydroxylase (TH) immunostaining revealed that the majority of c-Fos+ VTA neurons were TH-negative (Figure 1C; TH = 3.90%, non-TH = 96.1%). No significant increase in c-Fos expression was observed in the rostromedial tegmental nucleus (RMTg) (Figure S1). The VTA is a heterogeneous nucleus, and the largest neural population, excluding DA+ neurons, is GABAergic neurons (Dobi et al., 2010).

To confirm the recruitment of GABA+ neurons in the VTA during the LS and to investigate the dynamics of such activation, we carried out *in vivo* calcium imaging in the VTA using fiber photometry (Kim et al., 2016). Genetically encoded $Ca^{2+}$ indicators (GCaMP6s) (Figure 1D) or GFP were expressed in VTA$^{GABA+}$ neurons following stereotaxic infusions of the virus AAV-*EF1α*::DIO-GCaMP6s into the VTA of *GAD2*::Cre transgenic mice. VTA$^{GABA+}$ neurons showed significant activation of GCaMP6s activity following upper-field LS exposure (Figures 1E, S2D, and S2E; 6.16%, ΔF/F mean), whereas no signal change was observed in control mice expressing GFP (Figures S2A–S2C) or in those exposed to a control visual stimulus (Figures S3A–S3D).

Calcium signals from VTA$^{GABA+}$ neurons rose rapidly with the onset of looming (latency = 0.73 ± 0.15 s, mean ± SEM) and decayed slowly following LS offset (decay time constant = 3.19 ± 0.20 s) (Figure 1G). The activity of these calcium signals preceded the onset of flight behavior by 1.1 s (Figures 1E and 1F). Analysis revealed that the onset of the GCaMP6 transient signal was correlated with the onset of flight behavior (Figures 1H; linear regression R = 0.7094, ****$p < 0.0001$). The temporal dynamics of the calcium signals correlated well with that of looming-evoked flight-to-nest behaviors.

These data demonstrate that VTA$^{GABA+}$ neurons are recruited by exposure to LS and suggest that they may be involved in mediating defensive responses.

### VTA$^{GABA+}$ Neurons Mediate Looming-Evoked Defensive Behaviors

To determine whether the VTA has a role in looming-induced defensive behavior, we selectively suppressed neural activity in VTA$^{GABA+}$ neurons using optogenetic techniques. *GAD2*::Cre transgenic mice were bilaterally infected with AAV-*EF1α*::DIO-eNpHR3.0-mCherry to selectively express the light-activated chloride pump halorhodopsin (NpHR) in VTA$^{GABA+}$ neurons (Figures 2A and 2B). Delivery of continuous yellow light to the VTA of these mice significantly suppressed defensive behavior elicited by the LS compared with those infected with a control virus (AAV-*EF1α*::DIO-mCherry). This included an increased latency to return to nest, decreased speed of flight, and decrease in the percentage of hiding time spent in the nest after flight (latency: mCherry 4.6 ± 1.13 s versus NpHR 27.7 ± 10.05 s; speed: mCherry 1,015% ± 310.7% versus NpHR 220.5% ± 68.44%; hiding time: mCherry 69.5% ± 7.54% versus NpHR 25.17% ± 6.02%; Figures 2C and 2D). These data suggest that neural activity in VTA$^{GABA+}$ neurons is essential for defensive behavior to LS.

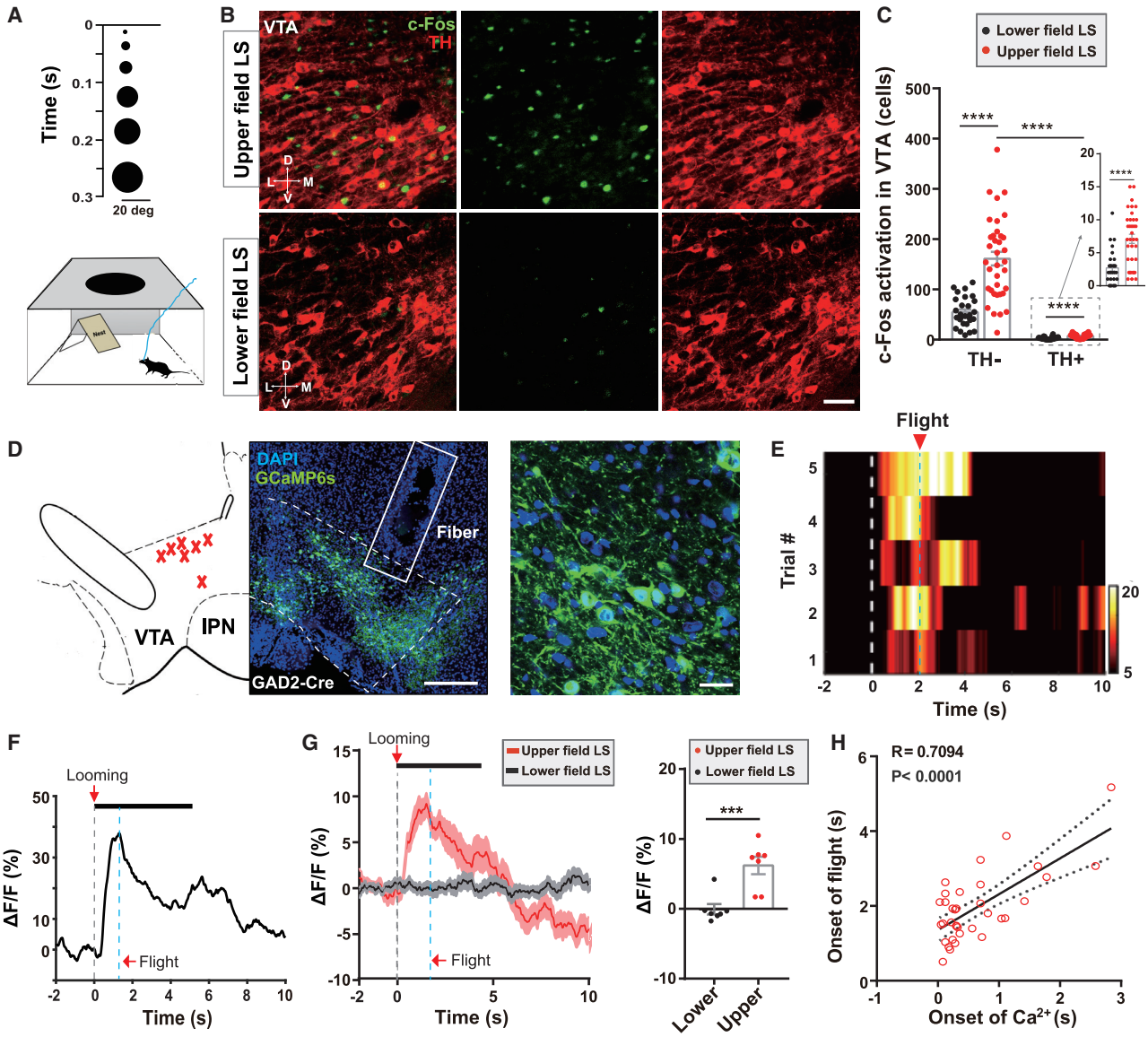


**Figure 1. VTA$^{GABA+}$ Neurons Respond to LS, which Evokes Defensive Behaviors**

(A) Schematic paradigm of an upper-field LS in a nest-containing open field apparatus.

(B) Representative images of c-Fos expression in the VTA following an upper-field LS (top) and lower-field LS (bottom) control stimulus (green, c-Fos; red, TH; scale bar, 100 μm).

(C) An upper-field LS led to higher c-Fos expression in VTA TH-negative neurons compared with a lower-field LS (n = 28–36 slices from 3 mice per group; TH-negative cells versus TH+ cells, $t_{70}$ = 11.31, ****p < 0.0001; for TH-negative cells, $t_{62}$ = 6.57, ****p < 0.0001; for TH+ cells, $t_{62}$ = 4.909, ****p < 0.0001; unpaired Student's t test).

(D) Left: schematic showing recording sites within the VTA; each red cross represents the optical fiber tip location from one mouse (n = 7 mice). Center: representative image of AAV-*EF1a*::DIO-GCaMP6s expression in the VTA of GAD2-Cre mice (scale bar, 250 μm). Right: high-magnification image showing AAV-*EF1a*::DIO-GCaMP6s expression (scale bar, 20 μm).

(E) Representative trial-by-trial heatmap presentation of calcium transients evoked by an upper-field LS in 5 trials from one mouse (white dotted line, onset of looming; blue dotted line, average latency of onset of flight).

(F) Representative peri-event plot of the 1 trial of calcium transients (black bar, presentation of the LS; gray dotted line: onset of looming; blue dotted line, latency of onset of flight).

(G) Left: average calcium transients for the entire test group (red line, upper-field LS; black line, lower-field LS). Shaded areas around means indicate error bars; the gray dotted line indicates onset of looming. Right: plot showing that there were more calcium transients during the upper-field LS than the lower-field LS ($n_{\text{Upper field LS}}$ = 7 mice; $n_{\text{Lower field LS}}$ = 7 mice, $t_{12}$ = 4.329, p = 0.001, unpaired Student's t test). Gray dotted line, onset of looming; blue dotted line, average of latency of onset of flight from all mice.

(H) Correlation analysis revealing that the onset of GCaMP6 transients was correlated with the onset of flight behavior (($n_{\text{Upper field LS}}$ = 35 trials from 7 mice, linear regression $R$ = 0.7094, $F_{1, 33}$ = 33.44, ****$p$ < 0.0001).

All data are presented as mean ± SEM.

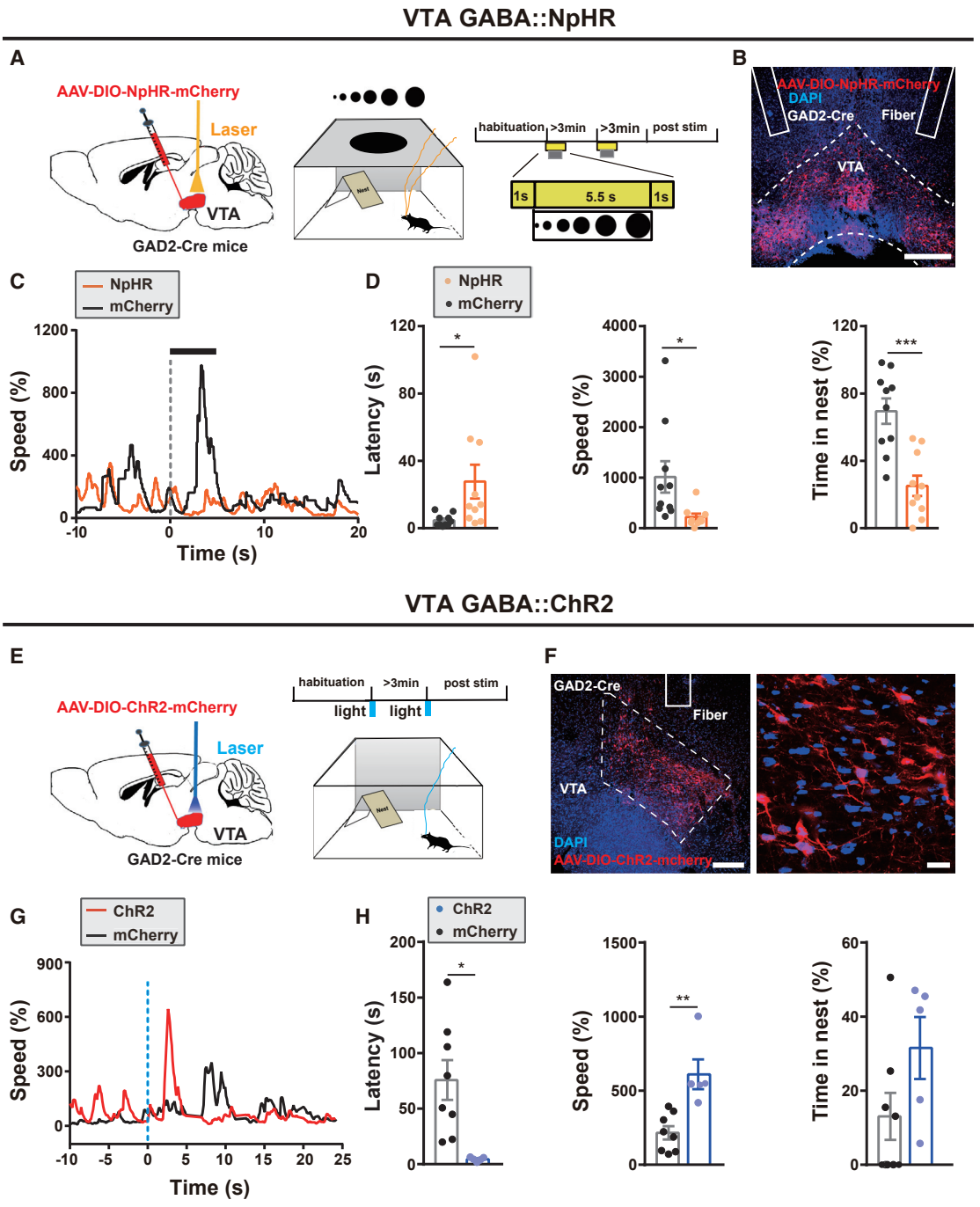


**Figure 2. VTA$^{GABA+}$ Neurons Mediate Looming-Evoked Defensive Behaviors**

(A) Left: schematic diagram of bilateral optogenetic inhibition of VTA GAD2+ neurons during LS. Center: open field with nest looming apparatus. Right: looming test protocol.

(B) Representative image showing NpHR virus expression in the VTA of a GAD2 -Cre mouse and the position of the fiber track (blue, DAPI; red, NpHR-mCherry; scale bar, 250 μm; solid border lines, fiber tracks).

(C) Representative curves showing that bilateral inhibition of VTA $^{GABA+}$ neurons significantly decreases the instant speed compared with the control (blue dotted line, onset of looming stimulation).

(D) Photoinhibition of VTA GAD2+ neurons resulted in higher latency back into the nest, lower speed, and shorter total percentage of hiding time spent in the nest after the LS compared with mCherry controls ($n_{mCherry}$ = 10 mice, $n_{NpHR}$ = 9–10 mice; for latency, $t_{18}$ = 2.284, *p = 0.0347; for speed, $t_{17}$ = 2.372, *p = 0.0297; for time in nest, $t_{18}$ = 4.593, ***p = 0.0002; unpaired Student's t test).

(E) Schematic diagram showing unilateral optogenetic activation of VTA GAD2+ neurons.

*(legend continued on next page)*

We then tested whether activation of VTA$^{GABA+}$ neurons triggers flight-to-nest behavior. *GAD2*::Cre transgenic mice were unilaterally infected with AAV-*EF1α*::DIO-ChR2-mCherry to selectively express the light-activated cation channelrodopsin (ChR2) in VTA$^{GABA+}$ neurons (Figures 2E and 2F). Mice were placed into the LS apparatus without presentation of the LS. Selective illumination of the VTA with blue light (5-ms pulse, 60 Hz for 2.5 s) elicited 1.29 ± 0.46 s transient intermittent immobility followed by flight-to-nest behavior in ChR2-expressing but not control virus-infected animals and resulted in significantly lower latency to return to nest and increased flight speed (latency: mCherry 75.75 ± 17.96 s versus ChR2 4.46 ± 0.82 s; speed: mCherry 215.7% ± 44.9% versus ChR2 610.7% ± 100.7%; Figures 2G and 2H). Longer blue light stimulation (5-ms pulse, 60 Hz for 20 s) induced flight-to-nest behavior and hiding (mCherry 10.92% ± 6.98% versus ChR2 58.43% ± 7.06%; Figures S4A–S4C) in the ChR2 group. These results demonstrate that activation of VTA$^{GABA+}$ neurons can induce innate defensive behaviors.

## SC Inputs to the VTA Mediate Looming-Evoked Innate Defensive Behaviors

To investigate possible upstream sources of visual inputs to the VTA that might mediate LS responses, we examined mono-synaptic inputs to VTA$^{GABA+}$ neurons using rabies virus tracing (Watabe-Uchida et al., 2012; Wickersham et al., 2007). *GAD2*::Cre mice were coinfected with AAV-*EF1α*::DIO-RVG and AAV-*EF1α*::DIO-TVA-GFP in the VTA and, 3 weeks later, infected with pseudotyped and glycoprotein-deficient rabies virus (RV-EvnA-dG-dsRed) using the same coordinates (Figures 3A and 3B). After an additional week, mice were euthanized and examined for the distribution of upstream neurons that synapse onto VTA$^{GABA+}$ neurons. dsRed+ cells were identified in the SC, lateral habenula (LHb), dorsomedial PAG (dmPAG), dorsolateral and lateral PAG (dl and lPAG), and ventrolateral PAG (vlPAG) (Figures 3C and S5A–S5E; mean RV+ neurons per starter cell: SC, 87.06%; LHb, 120.5%; dmPAG, 15.45%; dl and lPAG, 60.24%; vlPAG, 42.06%), regions known to provide inputs to the VTA (Beier et al., 2015; Faget et al., 2016). For the SC, dsRed+ cells were enriched mainly in the intermediate layer (IL) and deep layer (DL) (Figures 3C and 3E; mean RV+ neurons per starter cell: superficial layer [SL], 0%; IL, 63.65%; DL, 56.95%). Notably, dsRed+ cells were rare in the lateral geniculate nucleus (LGN) and primary visual cortex (V1) (Figure S5D, mean RV+ neurons per starter cell: LGN, 0.061%; V1, 0.236%), which are involved in traditional visual processing pathways (Schneider, 1969). Based on emerging studies (Evans et al., 2018; Huang et al., 2017; Li et al., 2018; Salay et al., 2018; Shang et al., 2018; Wei et al., 2015; Zelikowsky et al., 2018; Zhao et al., 2014) showing that the SC plays a role in processing innate fear-related signals and execution of subsequent behavior outputs, we focused on VTA GABA neuron input from the SC. To test whether VTA$^{GABA+}$-projecting SC neuronal activation is present during visually evoked flight-to-nest behavior, we used the same RV-tracing technology to label SC cells that project to VTA$^{GABA+}$ neurons and examined the overlap with looming-induced c-Fos. Compared with the lower-field LS, an upper-field LS evoked high-level c-Fos overlap with retrograde labeling of SC neurons (Figures 3D and 3G). Consistent with our c-Fos experiment (Figure 1C), which showed that VTA$^{DA+}$ neurons were less activated by looming than VTA$^{GABA+}$ neurons, the c-Fos expression of VTA$^{GABA+}$-projecting SC neurons was preferentially activated by an upper-field LS compared with VTA$^{DA+}$-projecting SC neurons (Figures S6A–S6D). These data suggest that the SC is a pivotal source of vision-related direct inputs to VTA$^{GABA+}$ neurons.

Immunostaining revealed that the majority of VTA-projecting SC neurons in the IL and DL were $Ca^{2+}$/calmodulin-dependent protein kinase IIα+ (CaMKIIα+) (Figures 3C and 3F; mean ± SEM, 84.3% ± 3.23), suggesting that VTA$^{GABA+}$ neurons received direct monosynaptic CaMKIIα+ inputs from the IL and DL of the SC.

Next we investigated whether direct SC inputs to the VTA might be functionally involved in looming-evoked defensive behavior. We selectively activated CaMKIIα::SC-VTA projections by delivering blue light (5-ms pulse, 20 Hz for 2.5 s) to the VTA in mice unilaterally infected in the SC with AAV-CaMKIIα::ChR2-mCherry (Figures 4A and 4B) and placed into the LS apparatus without presentation of the LS. Photoactivation of this CaMKIIα::SC-VTA pathway induced 1.75 ± 0.36 s transient intermittent immobility, followed by robust flight-to-nest and hiding-in-nest behavior, demonstrated by a significantly higher flight speed, decreased latency to return to the nest, and increased percentage of hiding time spent in the nest (latency: mCherry 31.53 ± 5.71 s versus ChR2 4.12 ± 0.94 s; speed: mCherry 212.5% ± 32.93% versus ChR2 451.5% ± 31.48%; hiding time: mCherry 29.76% ± 8.32% versus ChR2 81.02% ± 5.48%; Figures 4C, 4D, and S7B; Video S1) compared with the mCherry control group. Importantly, the defensive behavior was impaired by local pretreatment with a glutamate receptor antagonist (AP5/NBQX) into the VTA (Figures S7A), confirming a dependence of the behavioral effect on the activation of postsynaptic excitatory receptors in the VTA. CaMKIIα::SC-VTA projection activation also elicited significant increases in heart rate and circulating corticosterone levels (Figures S7C and S7D) compared with the control, suggesting widespread recruitment of downstream sympathetic arousal pathways. Direct photoactivation of CaMKIIα+ neurons in the IL and DL of the SC also resulted in flight-to-nest behavior (Figures S8A–S8F; Video S2). In our previous work, optogenetic activation of neurons in the medial-intermedial layer of the SC to the lateral posterior of the thalamus (LP) resulted in long-lasting freezing

(F) Representative image showing ChR2 virus expression in the VTA of a GAD2-Cre mouse and the position of the fiber track (blue, DAPI; red, ChR2-mCherry; scale bars, 20 μm and 250 μm, respectively; solid border line, fiber track).

(G) Representative curves showing significant instant speed evoked by opto-activation of VTA $^{GABA+}$ neurons compared with the control (blue dotted line, onset of blue light optical stimulation).

(H) 2.5-s photoactivation of VTA GAD2+ neurons induced flight-to-nest behavior, shown by a decrease latency of flight to nest, an increase in flight speed, and no change in total percentage of hiding time in the nest compared with mCherry controls ($n_{mCherry}$ = 8 mice, $n_{ChR2}$ = 5 mice; for latency, $t_{11}$ = 3.085, *p = 0.0104; for speed, $t_{11}$ = 4.089, **p = 0.0018; for time in nest, $t_{11}$ = 1.78, p = 0.1028; unpaired Student's t test).

All data are presented as mean ± SEM.

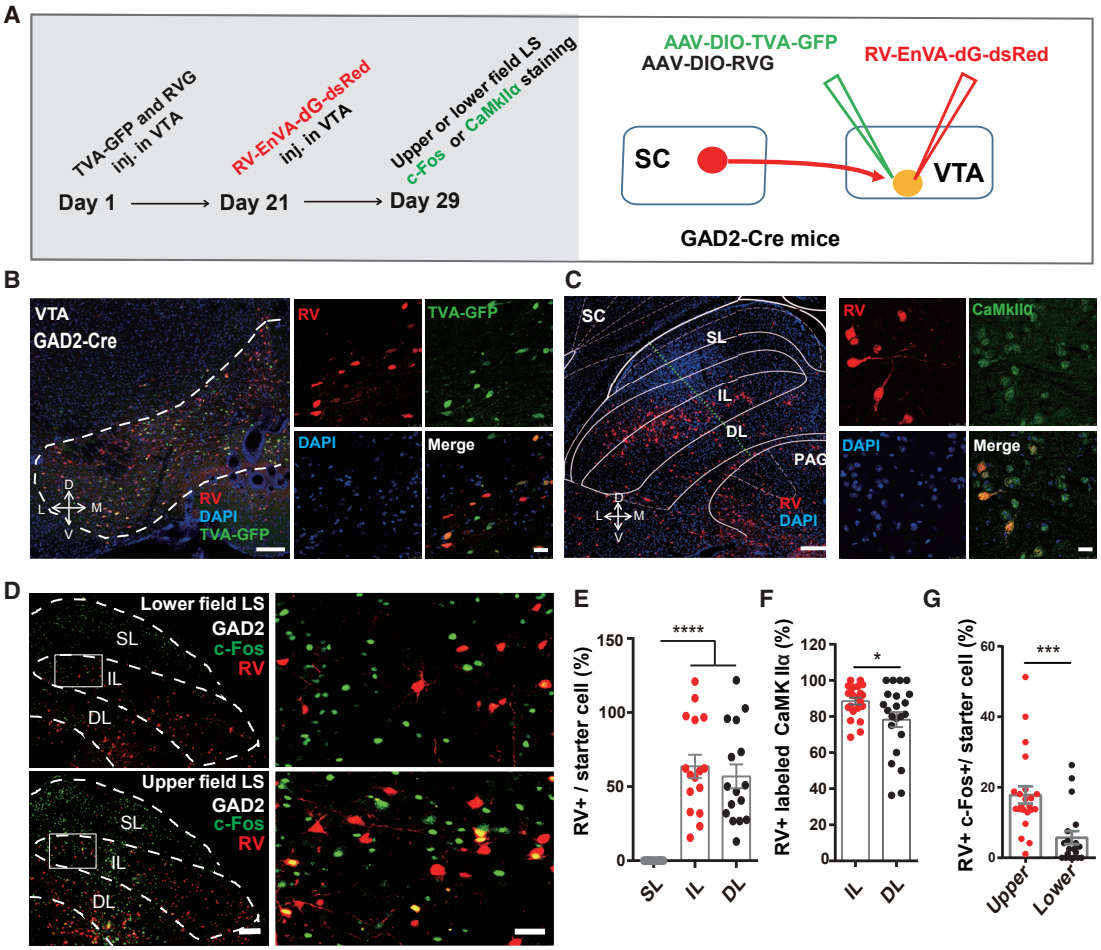


**Figure 3. VTA$^{GABA+}$ Neurons Receive Direct Monosynaptic CaMKIIα+ Inputs from the SC**

(A) Schematic of rabies virus-based cell type-specific monosynaptic tracing and c-Fos mapping of the looming protocol.

(B) Representative images denoting the starter cells in the VTA of GAD2-Cre mice (red, rabies-dsRed; green, TVA; blue, DAPI; scale bars, 250 μm and 25 μm, respectively).

(C) Representative images showing retrograde labeling in the SC with inputs to VTA GAD2+ neurons, co-labeled with CaMKIIα (red, rabies-dsRed; green, CaMKIIα; blue, DAPI; scale bars, 250 μm and 25 μm, respectively).

(D) Representative image showing rabies-dsRed-labeled neurons in the IL and DL of the SC in rabies virus-based GAD2+ neuron-specific monosynaptic tracing and c-Fos mapping following LS.

(E) Plot of rabies-dsRed+ neurons in the SC, showing that the intermediate and deep SC layers sent direct inputs to VTA $^{GABA+}$ neurons (SL, superficial layer; IL, intermediate layer; DL, deep layer; scale bars, 100 μm and 25 μm, respectively, n = 16 slices from 4 mice, $F_{2, 45} = 28.51$, ****$p < 0.0001$, one-way ANOVA).

(F) IL and DL of SC neurons sending inputs to VTA $^{GABA+}$ neurons; 84.3% ± 3.23% were CaMKIIα+ (n = 22 slices from 4 mice, $t_{42} = 2.254$, *p = 0.0294; unpaired Student's t test).

(G) Quantification of the percentage of rabies-dsRed-labeled neurons that overlap with c-Fos in the IL and DL of VTA starter cells ($n_{\text{lower field LS}}$ = 4 mice, $n_{\text{upper field LS}}$ = 5 mice, ***p = 0.0004, data presented as mean ± SEM; unpaired Student's t test).

behavior (Wei et al., 2015). In fact, we found here that the LP-projecting SC neurons are likely not the same population as VTA-projecting SC neurons using RV-mCherry injected into the LP and RV-EYFP injected into the VTA (Figure S9).

We then examined whether the CaMKIIα::SC-VTA pathway is essential for LS-evoked defensive responses. Mice were bilaterally infected with AAV-*CaMKIIa*::eNpHR 3.0-mCherry in the SC (Figure 4E). Selective delivery of continuous yellow light to the VTA of NpHR-expressing terminals elicited significant suppression of VTA putative non-DA neurons in the VTA (Figures 4G and 4I; light 258.5% ± 60.67% versus baseline −4.73% ± 20.71%). Compared with control virus-infected animals, photoinhibition of the CaMKIIα::SC-VTA pathway elicited a significant increase in latency to return to the nest, decreased the flight speed, and decreased the percentage of time spent in the nest after LS exposure (latency: mCherry 4.91 ± 0.63 s versus NpHR 48 ± 15.86 s; speed: mCherry 818.8% ± 175.1% versus NpHR 153.5% ± 26.82%; hiding time: mCherry 71.67% ± 6.62% versus NpHR 26.52% ± 5.37%; Figures 4J and 4K; Video S3). These data suggest that the CaMKIIα::SC-VTA pathway is essential for induction of innate defensive behaviors by LS.

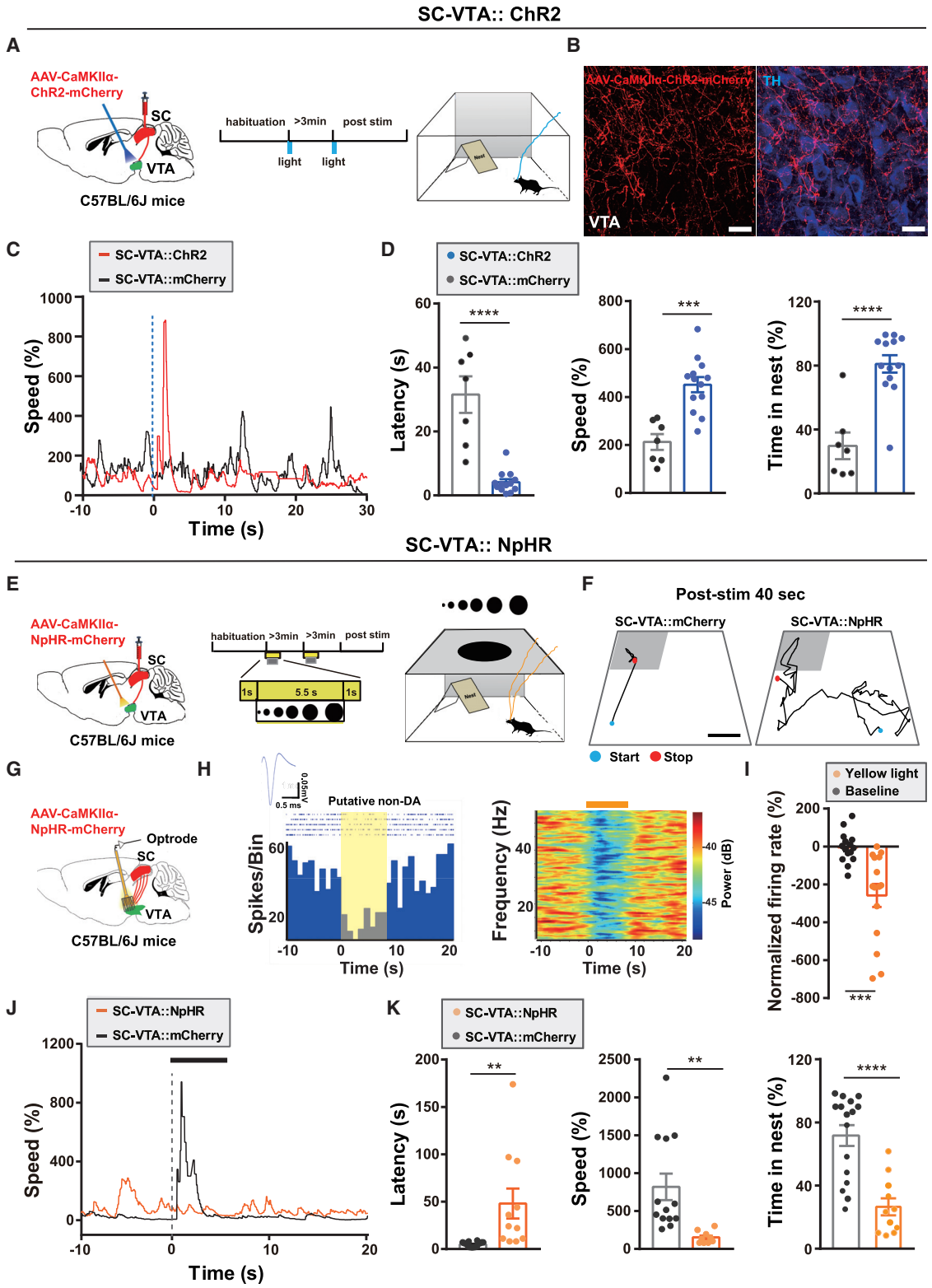


**Figure 4. The CaMKIIα::SC-VTA Pathway Mediates Looming-Evoked Defensive Behaviors**

(A) Left: schematic showing unilateral blue light stimulation of CaMKIIα$_{SC-VTA}$::ChR2. Center: stimulation protocol. Right: open field with nest looming apparatus. (B) Representative image showing ChR2 virus expression in fibers from SC CaMKIIα+ neurons in the VTA (red, AAV-CaMKIIα::ChR2-mCherry; blue, TH; scale bars, 25 μm).

*(legend continued on next page)*

### SC Glutamatergic Inputs Activate VTA$^{GABA+}$ Neurons

To understand the effect of LS on CaMKIIα::SC-VTA pathway activation, we performed *in vivo* and *in vitro* electrophysiology to examine neural activity in VTA$^{GABA+}$ neurons while activating CaMKIIα::SC-VTA inputs. *In vivo* multichannel extracellular recordings were carried out in mice following unilateral infection of the SC with AAV-CaMKIIα::ChR2-mCherry and selective delivery of blue light (5-ms pulse, 20 Hz) to the VTA. Among 97 VTA neurons recorded, the spike width, firing rate, and burst firing characteristics allowed us to classify 35 as putative non-DA+ (Figure 5D) and 62 as putative DA+ neurons (Figure S10B), although we need to bear in mind reports that, among putative VTA$^{DA+}$ neurons identified based on classical electrophysiological characteristics, a minority were non-DA+ neurons (Margolis et al., 2006; Ungless and Grace, 2012). For putative non-DA+ neurons, photostimulation of SC-VTA fibers resulted in time-locked firing with a mean latency of 5.65 ± 3.44 ms (Figure 5B). Most neurons (25 of 35, 71.4%) exhibited an increase in firing rate, whereas only a small fraction (2 of 35, 5.7%) exhibited a decrease (Figures 5C and 5D). The short latency of the responses confirmed our retrograde tracing data showing that a majority of VTA$^{GABA+}$ neurons receive direct excitatory SC inputs.

To better understand the functional properties of SC inputs to VTA$^{GABA+}$ neurons, we carried out *in vitro* whole-cell recordings in brain slices of *GAD2*::Cre transgenic mice infected unilaterally with AAV-CaMKIIα::ChR2-mCherry in the SC and AAV-*EF1α*::DIO-EYFP in the VTA (Figure 5E). Photostimulation of CaMKIIα::SC-VTA projections evoked excitatory postsynaptic currents (EPSCs) in VTA$^{GABA+}$ neurons that were eliminated by pretreatment with glutamate receptor antagonists (AP5 and NBQX) (Figure 5F).

VTA$^{GABA+}$ neurons play an important role in modulating the activity and responsiveness of VTA$^{DA+}$ neurons (Bocklisch et al., 2013; Jennings et al., 2013a; Nieh et al., 2016; Tan et al., 2012), primarily by directly inhibiting the firing of DA+ neurons. To examine whether such local inhibition might play a role in LS responses, we carried out photostimulation of CaMKIIα::SC-VTA projections (blue light, 20 Hz) while performing extracellular single-unit recordings of putative VTA$^{DA+}$ neurons. Unexpectedly, we observed short latency (7.03 ± 3.84 ms) and time-locked firing of putative DA+ neurons following CaMKIIα::SC-VTA activation (Figures S10A and S10C). The majority of putative DA+ neurons (44 of 62, 71%) exhibited increased firing following stimulation (Figures S10B, S10D, and S10E) and a minority (10 of 62, 16.1%) exhibited a decrease (Figures S10B, S10F, and S10G).

Although the c-Fos activation of VTA$^{DA+}$ neurons was rather weak under a LS, and considering the above electrophysiological recording data, it was of interest to test the possible function of VTA$^{DA+}$ neurons in looming-evoked defensive behavior. *DAT*::Cre mice were infected with AAV-*EF1α*::DIO-ChR2-mCherry in the VTA (Figures S11A–S11C). Activation of VTA$^{DA+}$ neurons did not elicit flight-to-nest behavior in an open field without looming. We then examined whether VTA$^{DA+}$ neurons were essential for LS-evoked defensive responses. *DAT*::Cre mice were bilaterally infected with AAV-*EF1α*::DIO-eNpHR3.0-mCherry in the VTA (Figure S11D), and LS responses were measured during photoinhibition. Inhibition of VTA$^{DAT+}$ neurons did not induce significant change in latency to return to nest or flight speed and increased the percentage of time spent in the nest compared with mCherry mice (latency: mCherry 3.27 ± 0.52 s versus NpHR 2.98 ± 0.47 s; speed: mCherry 788.2% ± 187.8% versus NpHR 947.9% ± 108.8%; hiding time: mCherry 66.26% ± 7.35% versus NpHR 88.34% ± 4.82%; Figures S11E and S11F). These data demonstrate the functional involvement of VTA$^{GABA+}$ neurons, but not VTA$^{DA+}$ neurons, in looming-evoked flight-to-nest behavior.

To test the possibility that influence from local GABAergic neurons led to the inhibition of VTA$^{DA+}$ neurons and that this led to the flight-to-nest behavior observed following the LS, we tested whether the looming-evoked defensive responses would be impaired following photo-activation of VTA$^{DA+}$ neurons. *DAT*::Cre mice were bilaterally infected with AAV-*EF1α*::DIO-ChR2-mCherry in the VTA (Figures S12A and S12B), and LS responses were measured during photostimulation. Activation of VTA$^{DAT+}$ neurons did not induce any noticeable change in latency to return to nest, flight speed, or percentage of time spent in the nest compared with mCherry mice (Figures S12C and S12D). Photoinhibition of VTA$^{DAT+}$ neurons without presentation of LS did not induce instant flight-to-nest behavior in an open field with a nest (Figures S12E–S12G). These data, together with the low

(C) Example of instant speed, highlighting the evoked flight behavior by opto-activation of CaMKIIα$_{SC-VTA}$::ChR2 compared with the mCherry control (blue dotted line, onset of blue light optical stimulation).
(D) Photoactivation of CaMKIIα$^{SC-VTA}$::ChR2 resulted in flight-to-nest behavior; specifically, an increase in speed, shorter latency back into the nest, and higher total percentage of time spent in the nest after the LS ($n_{mCherry}$ = 7 mice, $n_{ChR2}$ = 13 mice; for latency, $t_{18}$ = 6.394, ****p < 0.0001; for speed, $t_{18}$ = 0.4834, ***p = 0.0001; for time in nest, $t_{18}$ = 5.326, ****p < 0.0001; unpaired Student's t test).
(E) Left: schematic of bilateral optogenetic stimulation of CaMKIIα$^{SC-VTA}$::NpHR. Center: looming test protocol. Right: open field with nest looming apparatus.
(F) Representative motions tracks of two mice, showing that optogenetic activation of CaMKIIα$_{SC-VTA}$::NpHR resulted in less looming-evoked flight-to-nest behavior in the open field with the nest apparatus compared with mCherry controls.
(G) Schematic showing *in vivo* multichannel recording of single-unit VTA neuronal activity during optical inhibition of CaMKIIα SC-VTA terminals.
(H) Putative non-DA neuron suppressed using photoinhibition of CaMKIIα SC-VTA terminals, time-locked to 7.5 s photoinhibition. Left: representative peristimulus time histogram (PSTH) and raster plot of a single putative non-DA neuron. Right: local filed potential (LFP) activity in a VTA putative non-DA neuron (yellow bar, terminal stimulation period).
(I) Quantification of normalized firing rates of VTA putative non-DA neurons during inhibition of SC-VTA terminals (n = 15 units from 5 mice; $t_{14}$ = 4.172, ***p = 0.0009, paired Student's t test).
(J) Representative curves showing the instant speed significantly decreased by light inhibition of the CaMKIIα$^{SC-VTA}$ pathway compared with the mCherry control (gray dotted line, onset of looming stimulation).
(K) Optogenetic activation of CaMKIIα$^{SC-VTA}$::NpHR led to higher latency back into the nest, lower speed, and lower total percentage of time spent in the nest after the LS ($n_{mCherry}$ = 13–16 mice, $n_{NpHR}$ = 9–11 mice; for latency, $t_{25}$ = 3.303, **p = 0.0029; for speed, $t_{25}$ = 3.121, **p = 0.0054; for time in nest, $t_{25}$ = 4.927, ****p < *0.0001*; unpaired Student's t test).
All data are presented as mean ± SEM.

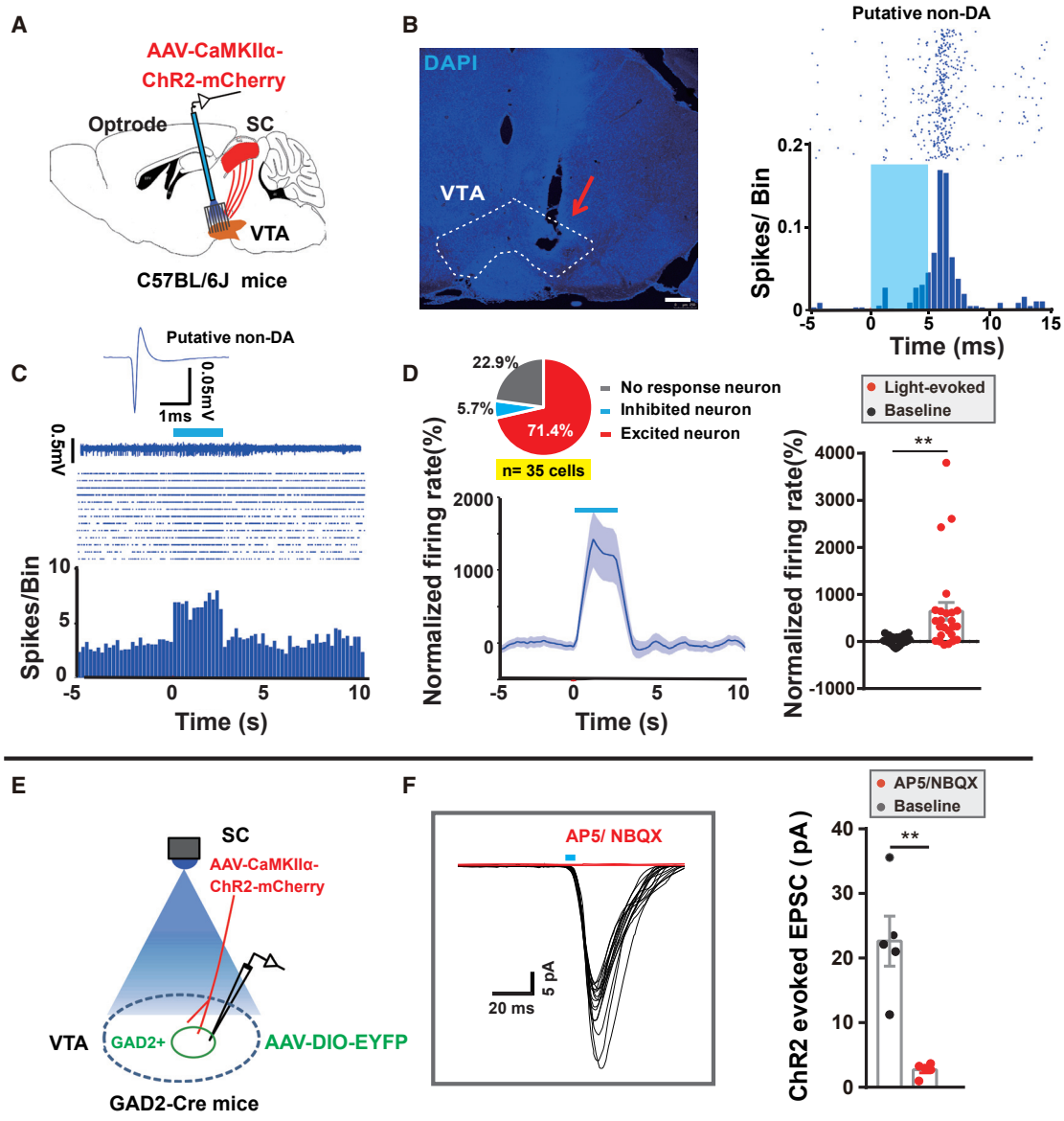


**Figure 5. SC Glutamatergic Inputs Activate VTA$^{GABA+}$ Neurons**

(A) Schematic showing *in vivo* multichannel recording of single-unit VTA neuronal activity while optically stimulating CaMKIIα SC-VTA terminals.

(B) Left: representative image showing optrode position in the VTA (arrow; scale bar, 250 μm). Right: representative PSTH and raster plot of a single neuron activated by CaMKIIα SC-VTA terminal stimulation, time-locked to 5 ms photostimulation (blue bar, terminal stimulation period).

(C) Example PSTH and raster plot of a putative VTA non-DA neuron excited by CaMKIIα SC-VTA terminal optogenetic stimulation for a total period of 2.5 s.

(D) Left: following terminal stimulation, 25 of 35 putative non-DA neurons (71.4%) were excited, 2 (5.7%) were inhibited, and 8 (22.9%) were unresponsive. Right: quantification of the normalized firing rate of putative non-DA neurons (n = 35 units from 7 mice; $t_{24}$ = 3.374, **p = 0.0025, paired Student's t test).

(E) Recording of evoked excitatory postsynaptic currents (eEPSCs) in VTA GAD2+ neurons using patch-clamp slice recording during optogenetic stimulation of the CaMKIIα SC-VTA terminals. AAV-*EF1a*::DIO-EYFP injections in GAD2-Cre mice used to visualize GAD2+ neurons.

(F) EPSCs in VTA GAD2+ neurons induced by CaMKIIα SC-VTA terminal light stimulation were not observed following injections of a glutamate receptor antagonist (AP5 and NBQX) (n = 5 cells from 4 mice, *p = 0.0078, $t_4$ = 4.936, paired Student's t test).

percentage of DA neurons that were inhibited by photostimulation, suggests that there is likely an alternative path to local inhibition of DA neurons that VTA$^{GABA+}$ neurons use to mediate looming-evoked flight behavior.

Whole-cell recordings in brain slices from *TH*::Cre mice in which photostimulation of CaMKIIα::SC-VTA projections was carried out confirmed the presence of evoked EPSCs (eEPSCs) and evoked inhibitory postsynaptic currents (eIPSCs) in VTA TH+ neurons (Figures S10H–S10M). Notably, only 4 of 21 cells (19%) showed eIPSCs, confirming a relatively low probability of inhibition of DA+ neurons following CaMKIIα::SC-VTA pathway stimulation (Figure S10N).

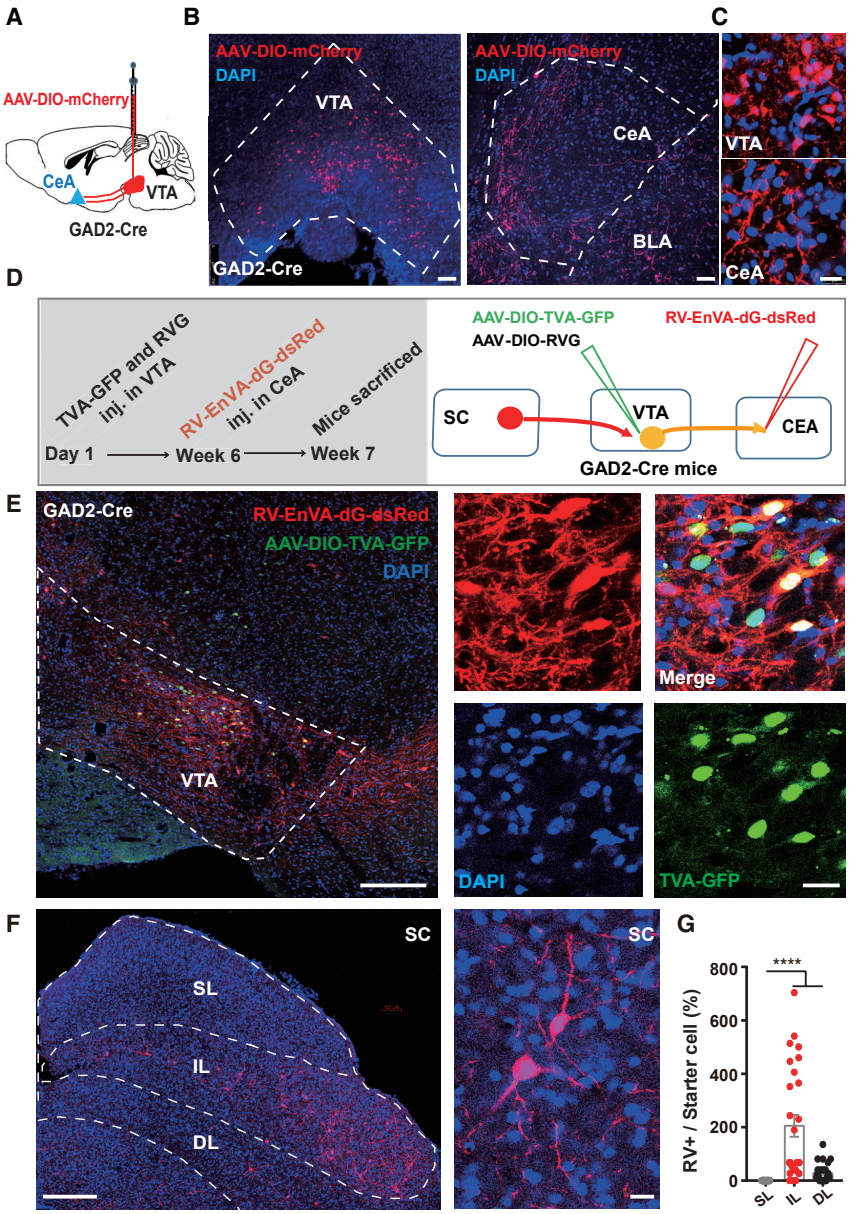


**Figure 6. Output-Specific Monosynaptic Viral Tracing Identifies the Input-Output Relationship of VTA$^{GABA+}$ Neurons**

(A) Schematic showing AAV-*EF1a*::DIO-mCherry injection into the VTA of GAD2-Cre mice.

(A and B) Representative coronal image showing targeted AAV-mCherry expression in the VTA (scale bars, 100 μm; B) and GAD2+ VTA-CeA terminals in the CeA (scale bars, 10 μm; C).

(D) Schematic showing tracing of the input-output relationships between VTA $^{GABA+}$ neurons. Rabies-EnVA-dG-dsRed virus was injected into the CeA. AAV-*EF1a*::DIO-RVG and AAV-*EF1a*::DIO-TVA-GFP were co-injected into the VTA of GAD2-Cre mice.

(E) Representative images showing VTA $^{GABA+}$ starter cells (blue, DAPI; red, RV-EnVA-dG-dsRed; green, AAV-TVA-GFP; yellow, VTA GAD2+ starter cells; scale bars, 250 μm and 10 μm, respectively).

(F) Representative images showing a substantial rabies-dsRed signal from CeA-projecting VTA$^{GABA+}$ neurons in the SC (blue, DAPI; red, rabies-dsRed; IL and DL; scale bars, 250 μm and 10 μm, respectively).

(G) Left: quantification of the number of rabies-dsRed-labeled neurons in subregions of the SC: the IL, the DL, and the SL (n = 27 slices from 3 mice; ****p < 0.0001; $F_{2, 78}$ = 18.5; one-way ANOVA).

All data are presented as mean ± SEM.

In summary, our structural and functional results derived from viral tracing and electrophysiological recordings, respectively, show that VTA$^{GABA+}$ neurons received functional glutamatergic inputs from the SC and that activation of this pathway led to activity of VTA$^{GABA+}$ neurons.

## CeA Is a Downstream Target of the SC-VTA GABAergic Pathway, and It Is Involved in Defensive Behavior

Next, we sought to identify downstream targets of VTA$^{GABA+}$ neurons that might mediate looming-evoked defense. Following infection of *GAD2*::Cre mice in the VTA with AAV-*EF1α*::DIO-mCherry (Figure 6A), dense labeled terminals were found in several brain regions, including the CeA, lateral hypothalamus (LH), LHb, and PAG (Figures 6B, 6C, and S13B–S13D). Because the CeA plays a critical role in mediating both learned and innate defensive behaviors (Gross and Canteras, 2012; Isosaka et al., 2015; LeDoux and Daw, 2018; Zelikowsky et al., 2018), we examined these projections further using output-specific monosynaptic viral tracing (Gielow and Zaborszky, 2017).

*GAD2*::Cre mice were infected with AAV-*EF1α*::DIO-histone-TVA-GFP and AAV-*EF1α*::DIO-RV-G in the VTA and RV-EnvA-dG-dsRed in the CeA 6 weeks later (Figures 6D and 6E). Consistent with monosynaptic rabies tracing data, histological analysis revealed frequent dsRed+ cell bodies in the IL and DL of the SC (Figures 6F and 6G), LHb, and PAG (Figures S5H and S5I) and only rare labeling in the LGN and V1 (Figure S5G; mean RV+ per starter cell: SC, 234.1%; LHb, 1101%; dmPAG, 188.5%; dl and lPAG, 300.4%; vlPAG, 406%).

Next we attempted to confirm the existence of a functional VTA-CeA circuit using whole-cell electrophysiological recordings in brain slices. *GAD2*::Cre mice were infected with AAV-*EF1α*::DIO-ChR2-mCherry in the VTA, and possible blue light-evoked IPSC responses were recorded in the CeA (Figures 7A and 7B). In the medial CeA (CeM), the majority of cells (7 of 10 cells, 70%) showed evoked IPSCs, whereas no evoked IPSCs were detected in the lateral CeA (CeL, 0 of 21 cells, 0%) (Figures 7C and 7D). Transient activation of VTA-CeA GABAergic pathway elicited a significant increase in the frequency of IPSCs during and after light stimulation (Figures 7C and 7E).

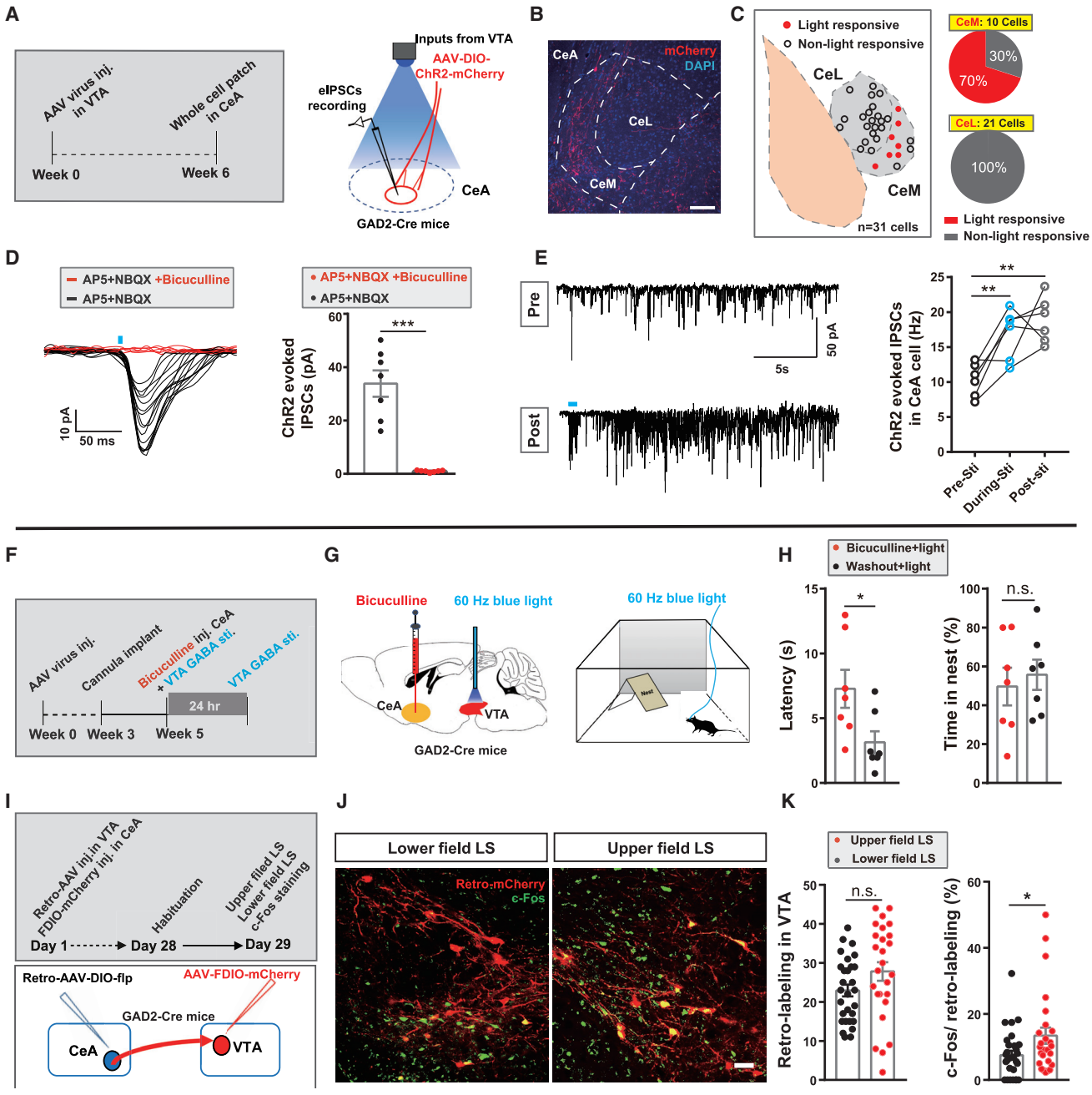


**Figure 7. The CeA, as a Downstream Target of the SC-VTA GABA Pathway, Is Involved in Looming-Evoked Flight-to-Nest Behavior**

(A) Schematic showing the timeline of recording of light-evoked inhibitory postsynaptic currents (eIPSCs) in CeA neurons using patch-clamp recording during optogenetic stimulation of GABAergic VTA-CeA terminals.

(B) Representative coronal image showing the GAD2+ VTA-CeA terminals in the CeM subregion of the CeA (scale bar, 100 μm).

(C) Location of recordings in the CeA. 21 of 31 cells recorded were located in the CeL, and 10 cells were located in the CeM. In the CeM, eIPSCs were recorded in 70% of cells (7 of 10 cells), and 30% were non-responsive, whereas all 21 cells in the CeL were non-responsive.

(D) The GABA-A receptor antagonist bicuculline abolished the IPSCs recorded in the CeA induced by GABAergic VTA-CeA terminal optical stimulation (n = 7 cells from 6 mice; data presented as mean ± SEM, ***p = 0.0006, $t_6$ = 6.625, Paired Student's t test)

(E) Left, light-induced increase of CeA neuronal eIPSCs frequency from brain slice patch clamp recordings; Right, quantification of eIPSCs frequency (n = 6 from 6 mice, Pre versus During: **p = 0.0086, $t_5$ = 4.188; Pre versus Post: **p = 0.0015, $t_5$ = 6.265; During versus Post: p = 0.4142, $t_5$ = 0.8901, paired Student's t test).

(F and G) Schematic experimental timeline (F) and schematic diagram of the behavioral paradigm (G). Shown is activation of VTA GABA neurons following inhibition of the CeA by injection of the GABA-A antagonist bicuculline.

*(legend continued on next page)*

Importantly, evoked IPSCs were eliminated by treatment of the slice with the GABA-A receptor antagonist bicuculline (Figure 7D), confirming that inhibition of the CeA by VTA$^{GABA+}$ neurons is mediated by GABA.

To test whether inhibition of the CeA plays a role in looming-evoked defensive behavior, we delivered the GABA-A receptor antagonist bicuculline directly into the CeA via pre-implanted guide cannulas 30 min before exposure to LS (Figures S14A and S14B). Bicuculline-treated animals had a significantly higher latency to return to the nest and no significant difference in hiding time in the nest compared with vehicle-treated control animals (Figure S14C), arguing for a critical role of inhibition in the CeA in visually evoked defensive responses. To further confirm that GABAergic signaling in the CeA mediates defensive responses evoked by photoactivation of VTA$^{GABA+}$ neurons, the GABA receptor antagonist (bicuculline) was delivered via pre-implanted guide cannulas into the CeA 30 min before exposure to a light stimulus (Figures 7F and 7G). Treated mice showed a significantly higher latency to return to the nest and no significant difference in nest hiding time compared with vehicle-treated mice, in which the drugs had been allowed to wash out (Figure 7H).

To precisely characterize possible involvement of CeA-projecting VTA$^{GABA+}$ neurons in looming-evoked flight behavior, we used retro-AAV to label the CeA-projecting VTA GABAergic neurons and examined the overlap with looming-induced c-Fos (Figure 7I). An upper-field LS led to significantly higher c-Fos expression in CeA-projecting VTA GABAergic neurons compared with a lower-field LS (Figure 7K).

In summary, these data from tracing, slice recording, and behavioral experiments indicate that VTA$^{GABA+}$ inhibitory inputs to the CeA are likely functionally involved in looming-evoked defense.

## DISCUSSION

In the current study, we found that exposure to a predator-like LS is associated with rapid activation of VTA$^{GABA+}$ neurons and that this activation is essential for LS-evoked defensive responses. Not only that, but activation of the same neurons elicits looming-like defensive behaviors. Neural tracing experiments revealed that the circuit responsible for this behavior includes a pathway from the SC to the VTA and then on to the CeA, suggesting that VTA$^{GABA+}$ neurons serve as a critical conduit in the integration of visual threat information with responses to aversive visual information.

The SC is sensitive to unexpected biological stimuli and has a functional role in detecting transient rather than static visual features (Redgrave and Gurney, 2006). A recent study has identified that the deep layers of the medial superior colliculus (dmSC) encode visual threatening stimuli (Evans et al., 2018), which were normally recognized as unexpected sensory events. The pathway from SC-VTA that processes unexpected biological saliency (Comoli et al., 2003; Dommett et al., 2005) has been identified using electrophysiological recording and rabies tracing (Dommett et al., 2005; Faget et al., 2016; Watabe-Uchida et al., 2012). Our viral tracing data, together with functional studies including *in vivo* multichannel recording and acute brain slice recording, complement this previous work and add clarity by directly demonstrating that VTA$^{GABA+}$ neurons receive monosynaptic glutamatergic inputs from the intermedial layer and deeper layer of superior colliculus (IDSC; Figure 3), which includes the dmSC.

We identified that the SC-VTA pathway mediates innate defensive behaviors evoked by a visual threat. We found that photostimulation of IDSC glutamatergic terminals of this population that project to the VTA induces transient intermittent immobility, followed by flight-to-nest and hiding-in-nest behavior, which mimics the behavioral responses associated with looming-evoked defense.

Previous studies have shown that VTA GABA neurons receive inputs from subcortical structures such as the SC, LHb, and PAG (Beier et al., 2015; Faget et al., 2016; Morales and Margolis, 2017). Aversive stimuli can induce activation of the bed nucleus of *stria terminalis* (BNST) projections to the VTA, and these can drive activation of VTA$^{GABA+}$ neurons (Jennings et al., 2013a). In our study, we found that VTA$^{GABA+}$ neurons mediate looming-evoked innate defensive responses through the glutamatergic pathway from the IDSC to the VTA. Fiber photometry recording revealed that VTA$^{GABA+}$ neurons became active following LS before flight and also during flight. Inhibition of VTA$^{GABA+}$ neurons significantly suppressed flight-to-nest behavior elicited by the LS, whereas activation of VTA$^{GABA+}$ neurons also triggered transient intermittent immobility followed by flight-to-nest behavior, similar to the behavior following activation of the glutamatergic pathway from the SC to the VTA. According to the economics hypothesis of flight from predators proposed by Ydenberg and Dill (1986), prey may be aware of the predator well before it decides to flee. Premature flight may actually lead to vulnerability because it may increase salience and draw the attention of the predator (Ydenberg and Dill, 1986). The transient intermittent immobility seems like "risk assessment-like" behavior, which may have a suitable temporal window to allow detection, evaluation, and preparation for making a decision to flee from the predator, all of which depend on

(H) Compared with the washout group (24 h after drug injection), microinjection of the GABA receptor antagonist bicuculline into the CeA resulted in higher latency to return to the nest and no change in the percentage of time spent in the nest (n = 7 mice; for latency, $t_6 = 2.78$, *p = 0.0320; for time in nest, $t_6 = 0.6298$, p = 0.5521; paired Student's t test).

(I) Schematic showing the CeA projecting VTA $^{GABA+}$ neurons activated by LS. Retro-AAV-*EF1a*::DIO-flp virus was injected into the CeA. AAV-*EF1a*::FDIO-mCherry virus was injected into the VTA of GAD2-Cre mice.

(J) Representative coronal image showing CeA-projecting VTA $^{GABA+}$ neurons (red) overlapped with c-Fos (green). Left: lower-field LS. Right: upper-field LS Scale bar, 25 μm.

(K) Left: quantification of the number of VTA retro-labeled GABA neurons. Right: quantification of the percentage of c-Fos expression in VTA retro-labeled GABA neurons. Black, lower-field LS; red, upper-field LS ($n_{\text{lower field LS}} = 29$ slices from 6 mice, $n_{\text{upper field LS}} = 26$ slices from 6 mice; p = 0.0832, $t_{53} = 1.765$; *p = 0.0353, $t_{53} = 2.16$; unpaired Student's t test).

All data are presented as mean ± SEM.

contextual factors, such as the existence of escape routes (Blanchard et al., 2011; Evans et al., 2018; Tovote et al., 2016). Taken together, our data suggest that survival in a threatening environment activates the glutamatergic pathway from SC to $VTA^{GABA+}$ neurons, which is involved in processing visual threats. $VTA^{GABA+}$ neurons could potentially process the incoming visual signal inputs from the SC and generate adaptive behavioral responses to threats based on saliency and motivational value. One major contribution of this study is the finding that $VTA^{GABA+}$ neurons are involved in processing potentially life-threatening innate fear signals.

Unexpected salient visual cues elicit an increase in the firing rate of DA+ neurons (Bromberg-Martin et al., 2010; Horvitz, 2000; Schultz, 1998), and visually evoked responses of $VTA^{DA+}$ neurons depend on inputs from the intermediate and deep layers of the SC (Dommett et al., 2005), which have been implicated in reinforcement learning and the habituation effect (Dommett et al., 2005; Redgrave and Gurney, 2006). Although we observed that $VTA^{GABA+}$ neurons were preferentially activated by upper-field LS compared with $VTA^{DA+}$ neurons, $VTA^{DA+}$ neurons were also activated, but to lesser extent (revealed by both the c-Fos experiment and *in vivo* and *in vitro* electrophysiological experiments). Consistent with previous work (Dommett et al., 2005), our study reveals that salient visual stimuli evoke a $VTA^{DA+}$ neuronal response through inputs from the SC. Here we predict that increased $VTA^{DA+}$ firing following activation of the CaMKIIα::SC-VTA pathway may contribute to reinforcement learning or a habituation effect.

Although activation of $VTA^{DA+}$ neurons was found, *in vivo* and *in vitro* electrophysiological experiments showed that photoactivation of CaMKIIα::SC-VTA led to inhibition of $VTA^{DA+}$ neurons (Figures S10F and S10K–S10N). Local GABA+ neurons are well known to modulate DA+ neuron excitability and firing (Bocklisch et al., 2013; Jennings et al., 2013a; Nieh et al., 2016; Tan et al., 2012). Consistent with this result, our c-Fos experiment (Figures 1A–1C and S6) showed that LS preferably activated $VTA^{GABA+}$ neurons over $VTA^{DA+}$ neurons. This preference is most likely caused by distinct SC neuronal populations that preferentially activate either $VTA^{GABA+}$ neurons or $VTA^{DA+}$ neurons (Figures S6). Two neural populations were classified by acute brain slice recording; one population significantly increased the IPSCs frequency in VTA TH+ during light stimulation, and another showed sustained inhibition after light stimulation (Figure S10L). DA neuron sustained inhibition seems to fit well with light-evoked long-term hiding behavior. Twenty-second photoactivation of $VTA^{GABA+}$ neurons that induced flight-to-nest behavior also led to a longer hiding time in the nest compared with 2.5-s photoactivation. This phenomenon may be due to increasing GABAergic excitation that results in stronger recruitment of inhibition of $VTA^{DA+}$ neurons, which may contribute to the modulation of hiding-in-nest behavior. To support this, we found that inhibition of $VTA^{DA+}$ neurons using NpHR during LS resulted in prolonged hiding time in the nest. In line with this finding, recent work shows that inhibition of VTA DA neuronal activity during foot shocks enhances fear (Luo et al., 2018).

In our study, we posit that inhibition of local $VTA^{GABA+}$ neurons on $VTA^{DA+}$ neurons might be involved in regulation of looming-induced defensive hiding behavior. An interesting experiment would be to characterize the electrophysiology of the interaction of $VTA^{GABA+}$ neurons and $VTA^{DA+}$ neurons during looming-evoked defensive responses in freely moving animals.

We found that 2.5-s activation of the CaMKIIα::SC-VTA pathway and $VTA^{GABA+}$ neurons elicited flight-to-nest behavior, whereas photoactivation of CaMKIIα::SC-VTA projections induced a longer hiding time in the nest compared with $VTA^{GABA+}$ neurons. Activation of the CaMKIIα::SC-VTA pathway most likely selectively evoked a specific subpopulation of $VTA^{GABA+}$ neurons that contributes to defensive responses. $VTA^{GABA+}$ neurons are well known to be involves in many behaviors (Bocklisch et al., 2013; Cohen et al., 2012; Jennings et al., 2013a; Nieh et al., 2016; Tan et al., 2012; van Zessen et al., 2012); therefore, activation of all $VTA^{GABA+}$ neurons (not specific) might result in a mixed effect on behavior and lead to a low-efficiency defensive response.

$VTA^{GABA+}$ neurons are heterogeneous subpopulations that include local GABA neurons and long-range GABA projection neurons (Morales and Margolis, 2017). Many reports have revealed roles of long-projecting GABAergic neurons in shaping behavioral outputs, such as feeding (Jennings et al., 2013b), avoidance (Lee et al., 2014), conditioned defensive behavior (Tovote et al., 2016), and innate defensive behavior (Chou et al., 2018). In addition, a role of VTA long-projecting GABAergic neurons in enhancing stimulus-outcome learning has been reported (Brown et al., 2012).

Next we explored the downstream targets of $VTA^{GABA+}$ neurons. Several brain regions, including the CeA, LH, LHb, and PAG, have terminals that project from $VTA^{GABA+}$ neurons. Given that the CeA plays a critical role in mediating both learned and innate defensive behaviors (Gross and Canteras, 2012; Isosaka et al., 2015; LeDoux and Daw, 2018; Zelikowsky et al., 2018), we tested the possible function of the VTA projecting GABA neurons to the CeA. We then examined these projections in further detail using output-specific monosynaptic viral tracing (Gielow and Zaborszky, 2017). Our tracing data demonstrated that $VTA^{GABA+}$ neurons sent long projections to the CeA and that these $VTA^{GABA+}$ neurons received monosynaptic inputs from the IDSC.

Although we did not observe obvious flight-to-nest behavior by direct activation of VTA-CeA GABAergic projections (data not shown), our retrograde tracing data demonstrated that CeA-projecting $VTA^{GABA+}$ neurons were significantly activated by upper-field LS (Figure 7J). It suggests that, among others, the CeA is possibly recruited by VTA GABA to execute visually evoked flight behavior.

Furthermore, acute patch-clamp slice recording shows that the $VTA^{GABA+}$ projections preferentially form functional connectivity with the CeM, the major output of the CeA that mediates defensive behavior output (Ciocchi et al., 2010; Haubensak et al., 2010; LeDoux et al., 1988; Tovote et al., 2016), but not the CeL. Recent reports show that the CeA is involved in conditioned flight behavior and that a competitive inhibitory circuit in the CeA facilitates the selection of freezing and flight behavior, where inhibition of the CeM leads to flight (Fadok et al., 2017; Terburg et al., 2018; Yu et al., 2016). This flight behavior likely originates downstream of the CeA in regions such as the PAG and hypothalamus (Fadok et al., 2017; Tovote et al., 2016; Gross

and Canteras, 2012). It is possible that looming-activated VTA$^{GABA+}$ neurons send long inhibitory projections to the CeM subregion, which would inhibit the CeM locally, promoting flight behavior over freezing behavior. Our results are consistent with previous studies (Isosaka et al., 2015; Kalin et al., 2004; Salay et al., 2018), indicating involvement of the CeA in flight behavior evoked by innate threats, suggesting possible overlapping neural circuit bases for innate threats and learned threat processing in the amygdala (Gross and Canteras, 2012; LeDoux and Daw, 2018). Given the accumulation of reports on amygdala involvement in defensive behaviors, including this study, it would be interesting to further investigate the mechanism underlying the relation of innate threats and learned threat processing. Although our data suggest that the CeA is an important downstream target for looming-activated VTA$^{GABA+}$ neurons, other downstream areas of VTA$^{GABA+}$ neurons, such as the PAG, LH, and LHb, which are well known to be important for defensive behaviors, may also be involved in looming-evoked defensive responses.

The selection and rapid execution of an appropriate defensive response, including quick detection of the salient environmental cue, successful flight to safety, and hiding, require the integration of multiple sensory information inputs, spatial memory, and adaptation to the environment. The IDSC plays an important role in integrating multiple sensory inputs from environmental stimuli to rapidly escape from potential danger (Stein et al., 2009). Pharmacological infusion and electric stimulation of the IDSC generate a broad spectrum of defensive responses, including orienting, flight, and freezing (Redgrave et al., 1981; Sahibzada et al., 1986). Very recently, Evans et al. (2018) identified that dmSC neurons that send projections to the dorsal periaqueductal gray matter (dPAG) encode threat stimuli and that, when their firing reaches a synaptic threshold at the dPAG, escape behavior is initiated (Evans et al., 2018). In our study, activation of IDSC glutamatergic neurons, which includes this area of the dmSC, and the IDSC-VTA pathway contributed to transient intermittent immobility and then flight-to-nest and hiding-in-nest behavior. The dmSC activity predicted the decision to flight 0.9 s before onset of flight, and dPAG neurons start to respond only after onset of flight (Evans et al., 2018). Our results show that VTA$^{GABA+}$ neurons were activated by the LS before flight (latency of looming-evoked onset of $Ca^{2+}$ signal of VTA$^{GABA+}$ neurons, 0.73 s; latency of looming-evoked onset of flight, 1.83 s) and sustained activity during flight.

The responses of VTA$^{GABA+}$ neurons before flight initiation likely indicated the response to threat inputs through the pathway from the IDSC to the VTA before initiation of the appropriate behavior. This evidence fits with the time course of the transient intermittent immobility response to the LS. Bearing in mind the potential gating role of GABA in filtering incoming inputs (Ren et al., 2012), our data suggest that the IDSC-to-VTA$^{GABA+}$ pathway carries visual threat inputs. Understanding how an animal assesses the risk and generates the most optimized option for defense through intrastimulus competition based on saliency and motivational value would be a very interesting future direction.

Our previous study demonstrated that glutamatergic neurons in medial part of intermedial layer of superior colliculus (mILSC) projected to an LP-lateral amygdala (LA) circuit mediating looming-evoked freezing behavior in an open field without a nest (Wei et al., 2015; Figures S9). Our current neural tracing results confirmed that CeA-projecting VTA$^{GABA+}$ neurons receive inputs from the IDSC. This study provides a potential anatomical basis for further research to disentangle the behavioral selection processes that occur within the amygdala during unconditioned and conditioned defensive responses.

A detailed mechanistic understanding of the neural basis of these circuits will provide new insights into the potential mechanisms of survival across species as well as the maladaptive behavior in fear- and anxiety-related mental disorders (Deisseroth, 2014; Lüthi and Lüscher, 2014; Pitman et al., 2012; Tovote et al., 2015).

## STAR★METHODS

Detailed methods are provided in the online version of this paper and include the following:

- KEY RESOURCES TABLE
- CONTACT FOR REAGENT AND RESOURCE SHARING
- EXPERIMENTAL MODEL AND SUBJECT DETAILS
  - Animals
- METHOD DETAILS
  - Viral vector preparation
  - Virus injection
  - *Trans*-synaptic tracer labeling
  - Implantation of optical fiber(s) and cannulas
- PATCH-CLAMP ELECTROPHYSIOLOGY
  - Histology, immunohistochemistry, and microscopy
  - Plasma corticosterone measurement
  - Electrocardiogram recording
  - Looming test
  - Optogenetic manipulation
- PHARMACOLOGICAL ANTAGONISM
  - Behavioral analysis
  - *In vivo* electrophysiology
  - Data analysis
  - Fiber Photometry
- DATA ANALYSIS
- QUANTIFICATION AND STATISTICAL ANALYSIS

### SUPPLEMENTAL INFORMATION

Supplemental Information can be found online at https://doi.org/10.1016/j.neuron.2019.05.027.

### ACKNOWLEDGMENTS

We thank Minmin Luo for providing the GAD2-ires-Cre mice, Zilong Qiu for TH-Cre mice, and Yangling Mu for DAT-ires-Cre mice. We thank Cornelius T. Gross for comments on our manuscript. We also thank Wei He, Tiaotiao Liu, and Mi Xia for conducting the electrophysiology analyses. This work was supported by National Natural Science Foundation of China (NSFC) 31630031 (to L.W.); NSFC 81425010 (to L.W.); NSFC 31471109 (to L.L.); NSFC 31671116 (to S.C.); NSFC 91632303/H09 (to F.X.); NSFC 91732304 (to G.B.); NSFC 31500861 (to P.W.); International Partnership Program of Chinese Academy of Sciences 172644KYS820170004 (to L.W.); Helmholtz-CAS joint research grant GJHZ1508 (to L.W.); Guangdong Provincial Key Laboratory of Brain Connectome and Behavior 2017B030301017 (to L.W.); Shenzhen government

grants JCYJ20160429190927063 (to X.L.), KQJSCX20160301144002 (to L.L.), JCYJ20170413164535041 (to L.W.), and JCYJ20150401150223647 (to Z. Zhou); Research Instrument Development Project of the Chinese Academy of Sciences YJKYYQ20170064 (to P.W.); Youth Innovation Promotion Association CAS 2017413 (to P.W.) and JSGG20160429190521240 (to F.Y.); Shenzhen Municipal Funding GJHZ20160229200136090 (to L.W.); Shenzhen Discipline Construction Project for Neurobiology DRCSM [2016]1379 (to L.W.); the Ten Thousand Talent Program (to L.W.); the Guangdong Special Support Program (to L.W.); and Science and Technology Planning Project of Guangdong Province 2018B030331001 (to L.W.).

## AUTHOR CONTRIBUTIONS

Conceptualization, Z. Zhou, X.L., and L.W.; Methodology, Z. Zhou, X.L., and L.W.; Formal Analysis, Z. Zhou, X.L.; Investigation, Z. Zhou, X.L., S.C., Z. Zhang., X.H., M.Q., Y.L., Y.T., P.W., N.L., R.S., J.L., and C.C.; Writing – Original Draft, Z. Zhou, X.L., and L.W.; Writing – Review & Editing, L.W., Z. Zhou, X.L., F.X., L.L.,G.B., and G.F.; Funding Acquisition, L.W. and F.X.; and Supervision, L.W. and F.X.

## DECLARATION OF INTERESTS

The authors declare no competing interests.

Received: September 17, 2018
Revised: March 11, 2019
Accepted: May 15, 2019
Published: June 12, 2019

## REFERENCES

Beier, K.T., Steinberg, E.E., DeLoach, K.E., Xie, S., Miyamichi, K., Schwarz, L., Gao, X.J., Kremer, E.J., Malenka, R.C., and Luo, L. (2015). Circuit Architecture of VTA Dopamine Neurons Revealed by Systematic Input-Output Mapping. Cell *162*, 622–634.

Blanchard, D.C., Griebel, G., Pobbe, R., and Blanchard, R.J. (2011). Risk assessment as an evolved threat detection and analysis process. Neurosci. Biobehav. Rev. *35*, 991–998.

Bocklisch, C., Pascoli, V., Wong, J.C.Y., House, D.R.C., Yvon, C., De Roo, M., Tan, K.R., and Lüscher, C. (2013). Cocaine disinhibits dopamine neurons by potentiation of GABA transmission in the ventral tegmental area. Science *341*, 1521–1525.

Brischoux, F., Chakraborty, S., Brierley, D.I., and Ungless, M.A. (2009). Phasic excitation of dopamine neurons in ventral VTA by noxious stimuli. Proc. Natl. Acad. Sci. USA *106*, 4894–4899.

Bromberg-Martin, E.S., Matsumoto, M., and Hikosaka, O. (2010). Dopamine in motivational control: rewarding, aversive, and alerting. Neuron *68*, 815–834.

Brown, M.T., Tan, K.R., O'Connor, E.C., Nikonenko, I., Muller, D., and Lüscher, C. (2012). Ventral tegmental area GABA projections pause accumbal cholinergic interneurons to enhance associative learning. Nature *492*, 452–456.

Chou, X.L., Wang, X., Zhang, Z.G., Shen, L., Zingg, B., Huang, J., Zhong, W., Mesik, L., Zhang, L.I., and Tao, H.W. (2018). Inhibitory gain modulation of defense behaviors by zona incerta. Nat. Commun. *9*, 1151.

Ciocchi, S., Herry, C., Grenier, F., Wolff, S.B., Letzkus, J.J., Vlachos, I., Ehrlich, I., Sprengel, R., Deisseroth, K., Stadler, M.B., et al. (2010). Encoding of conditioned fear in central amygdala inhibitory circuits. Nature *468*, 277–282.

Cohen, J.Y., Haesler, S., Vong, L., Lowell, B.B., and Uchida, N. (2012). Neuron-type-specific signals for reward and punishment in the ventral tegmental area. Nature *482*, 85–88.

Comoli, E., Coizet, V., Boyes, J., Bolam, J.P., Canteras, N.S., Quirk, R.H., Overton, P.G., and Redgrave, P. (2003). A direct projection from superior colliculus to substantia nigra for detecting salient visual events. Nat. Neurosci. *6*, 974–980.

Davis, K.L., Kahn, R.S., Ko, G., and Davidson, M. (1991). Dopamine in schizophrenia: a review and reconceptualization. Am. J. Psychiatry *148*, 1474–1486.

Deisseroth, K. (2014). Circuit dynamics of adaptive and maladaptive behaviour. Nature *505*, 309–317.

Dobi, A., Margolis, E.B., Wang, H.L., Harvey, B.K., and Morales, M. (2010). Glutamatergic and nonglutamatergic neurons of the ventral tegmental area establish local synaptic contacts with dopaminergic and nondopaminergic neurons. J. Neurosci. *30*, 218–229.

Dommett, E., Coizet, V., Blaha, C.D., Martindale, J., Lefebvre, V., Walton, N., Mayhew, J.E.W., Overton, P.G., and Redgrave, P. (2005). How visual stimuli activate dopaminergic neurons at short latency. Science *307*, 1476–1479.

Ekstrand, M.I., Terzioglu, M., Galter, D., Zhu, S., Hofstetter, C., Lindqvist, E., Thams, S., Bergstrand, A., Hansson, F.S., Trifunovic, A., et al. (2007). Progressive parkinsonism in mice with respiratory-chain-deficient dopamine neurons. Proc. Natl. Acad. Sci. USA *104*, 1325–1330.

Evans, D.A., Stempel, A.V., Vale, R., Ruehle, S., Lefler, Y., and Branco, T. (2018). A synaptic threshold mechanism for computing escape decisions. Nature *558*, 590–594.

Fadok, J.P., Krabbe, S., Markovic, M., Courtin, J., Xu, C., Massi, L., Botta, P., Bylund, K., Müller, C., Kovacevic, A., et al. (2017). A competitive inhibitory circuit for selection of active and passive fear responses. Nature *542*, 96–100.

Faget, L., Osakada, F., Duan, J., Ressler, R., Johnson, A.B., Proudfoot, J.A., Yoo, J.H., Callaway, E.M., and Hnasko, T.S. (2016). Afferent Inputs to Neurotransmitter-Defined Cell Types in the Ventral Tegmental Area. Cell Rep. *15*, 2796–2808.

Fields, H.L., Hjelmstad, G.O., Margolis, E.B., and Nicola, S.M. (2007). Ventral tegmental area neurons in learned appetitive behavior and positive reinforcement. Annu. Rev. Neurosci. *30*, 289–316.

Gielow, M.R., and Zaborszky, L. (2017). The input-output relationship of the cholinergic basal forebrain. Cell Rep. *18*, 1817–1830.

Gross, C.T., and Canteras, N.S. (2012). The many paths to fear. Nat. Rev. Neurosci. *13*, 651–658.

Haubensak, W., Kunwar, P.S., Cai, H., Ciocchi, S., Wall, N.R., Ponnusamy, R., Biag, J., Dong, H.W., Deisseroth, K., Callaway, E.M., et al. (2010). Genetic dissection of an amygdala microcircuit that gates conditioned fear. Nature *468*, 270–276.

Horvitz, J.C. (2000). Mesolimbocortical and nigrostriatal dopamine responses to salient non-reward events. Neuroscience *96*, 651–656.

Huang, L., Yuan, T., Tan, M., Xi, Y., Hu, Y., Tao, Q., Zhao, Z., Zheng, J., Han, Y., Xu, F., et al. (2017). A retinoraphe projection regulates serotonergic activity and looming-evoked defensive behaviour. Nat. Commun. *8*, 14908.

Isosaka, T., Matsuo, T., Yamaguchi, T., Funabiki, K., Nakanishi, S., Kobayakawa, R., and Kobayakawa, K. (2015). Htr2a-expressing cells in the central amygdala control the hierarchy between innate and learned fear. Cell *163*, 1153–1164.

Jennings, J.H., Sparta, D.R., Stamatakis, A.M., Ung, R.L., Pleil, K.E., Kash, T.L., and Stuber, G.D. (2013a). Distinct extended amygdala circuits for divergent motivational states. Nature *496*, 224–228.

Jennings, J.H., Rizzi, G., Stamatakis, A.M., Ung, R.L., and Stuber, G.D. (2013b). The inhibitory circuit architecture of the lateral hypothalamus orchestrates feeding. Science *341*, 1517–1521.

Kalin, N.H., Shelton, S.E., and Davidson, R.J. (2004). The role of the central nucleus of the amygdala in mediating fear and anxiety in the primate. J. Neurosci. *24*, 5506–5515.

Kim, C.K., Yang, S.J., Pichamoorthy, N., Young, N.P., Kauvar, I., Jennings, J.H., Lerner, T.N., Berndt, A., Lee, S.Y., Ramakrishnan, C., et al. (2016). Simultaneous fast measurement of circuit dynamics at multiple sites across the mammalian brain. Nat. Methods *13*, 325–328.

Kremer, E.J., Boutin, S., Chillon, M., and Danos, O. (2000). Canine adenovirus vectors: an alternative for adenovirus-mediated gene transfer. J. Virol. *74*, 505–512.

Lammel, S., Lim, B.K., Ran, C., Huang, K.W., Betley, M.J., Tye, K.M., Deisseroth, K., and Malenka, R.C. (2012). Input-specific control of reward and aversion in the ventral tegmental area. Nature *491*, 212–217.

LeDoux, J. (2012). Rethinking the emotional brain. Neuron *73*, 653–676.

LeDoux, J., and Daw, N.D. (2018). Surviving threats: neural circuit and computational implications of a new taxonomy of defensive behaviour. Nat. Rev. Neurosci. *19*, 269–282.

LeDoux, J.E., Iwata, J., Cicchetti, P., and Reis, D.J. (1988). Different projections of the central amygdaloid nucleus mediate autonomic and behavioral correlates of conditioned fear. J. Neurosci. *8*, 2517–2529.

Lee, A.T., Vogt, D., Rubenstein, J.L., and Sohal, V.S. (2014). A class of GABAergic neurons in the prefrontal cortex sends long-range projections to the nucleus accumbens and elicits acute avoidance behavior. J. Neurosci. *34*, 11519–11525.

Li, L., Feng, X., Zhou, Z., Zhang, H., Shi, Q., Lei, Z., Shen, P., Yang, Q., Zhao, B., Chen, S., et al. (2018). Stress accelerates defensive responses to looming in mice and involves a locus coeruleus-superior colliculus projection. Curr. Biol. *28*, 859–871.e5.

Luo, R., Uematsu, A., Weitemier, A., Aquili, L., Koivumaa, J., McHugh, T.J., and Johansen, J.P. (2018). A dopaminergic switch for fear to safety transitions. Nat. Commun. *9*, 2483.

Lüscher, C., and Malenka, R.C. (2011). Drug-evoked synaptic plasticity in addiction: from molecular changes to circuit remodeling. Neuron *69*, 650–663.

Lüthi, A., and Lüscher, C. (2014). Pathological circuit function underlying addiction and anxiety disorders. Nat. Neurosci. *17*, 1635–1643.

Margolis, E.B., Lock, H., Hjelmstad, G.O., and Fields, H.L. (2006). The ventral tegmental area revisited: is there an electrophysiological marker for dopaminergic neurons? J. Physiol. *577*, 907–924.

Matsumoto, M., and Hikosaka, O. (2009). Two types of dopamine neuron distinctly convey positive and negative motivational signals. Nature *459*, 837–841.

Mirenowicz, J., and Schultz, W. (1996). Preferential activation of midbrain dopamine neurons by appetitive rather than aversive stimuli. Nature *379*, 449–451.

Morales, M., and Margolis, E.B. (2017). Ventral tegmental area: cellular heterogeneity, connectivity and behaviour. Nat. Rev. Neurosci. *18*, 73–85.

Nestler, E.J., and Carlezon, W.A., Jr. (2006). The mesolimbic dopamine reward circuit in depression. Biol. Psychiatry *59*, 1151–1159.

Nieh, E.H., Vander Weele, C.M., Matthews, G.A., Presbrey, K.N., Wichmann, R., Leppla, C.A., Izadmehr, E.M., and Tye, K.M. (2016). Inhibitory input from the lateral hypothalamus to the ventral tegmental area disinhibits dopamine neurons and promotes behavioral activation. Neuron *90*, 1286–1298.

Pitman, R.K., Rasmusson, A.M., Koenen, K.C., Shin, L.M., Orr, S.P., Gilbertson, M.W., Milad, M.R., and Liberzon, I. (2012). Biological studies of post-traumatic stress disorder. Nat. Rev. Neurosci. *13*, 769–787.

Redgrave, P., and Gurney, K. (2006). The short-latency dopamine signal: a role in discovering novel actions? Nat. Rev. Neurosci. *7*, 967–975.

Redgrave, P., Dean, P., Souki, W., and Lewis, G. (1981). Gnawing and changes in reactivity produced by microinjections of picrotoxin into the superior colliculus of rats. Psychopharmacology (Berl.) *75*, 198–203.

Ren, Q., Li, H., Wu, Y., Ren, J., and Guo, A. (2012). A GABAergic inhibitory neural circuit regulates visual reversal learning in Drosophila. J. Neurosci. *32*, 11524–11538.

Sahibzada, N., Dean, P., and Redgrave, P. (1986). Movements resembling orientation or avoidance elicited by electrical stimulation of the superior colliculus in rats. J. Neurosci. *6*, 723–733.

Salay, L.D., Ishiko, N., and Huberman, A.D. (2018). A midline thalamic circuit determines reactions to visual threat. Nature *557*, 183–189.

Savitt, J.M., Jang, S.S., Mu, W., Dawson, V.L., and Dawson, T.M. (2005). Bcl-x is required for proper development of the mouse substantia nigra. J. Neurosci. *25*, 6721–6728.

Schneider, G.E. (1969). Two visual systems. Science *163*, 895–902.

Schultz, W. (1998). Predictive reward signal of dopamine neurons. J. Neurophysiol. *80*, 1–27.

Shang, C., Chen, Z., Liu, A., Li, Y., Zhang, J., Qu, B., Yan, F., Zhang, Y., Liu, W., Liu, Z., et al. (2018). Divergent midbrain circuits orchestrate escape and freezing responses to looming stimuli in mice. Nat. Commun. *9*, 1232.

Stein, B.E., Stanford, T.R., and Rowland, B.A. (2009). The neural basis of multisensory integration in the midbrain: its organization and maturation. Hear. Res. *258*, 4–15.

Tan, K.R., Yvon, C., Turiault, M., Mirzabekov, J.J., Doehner, J., Labouèbe, G., Deisseroth, K., Tye, K.M., and Lüscher, C. (2012). GABA neurons of the VTA drive conditioned place aversion. Neuron *73*, 1173–1183.

Taniguchi, H., He, M., Wu, P., Kim, S., Paik, R., Sugino, K., Kvitsiani, D., Fu, Y., Lu, J., Lin, Y., et al. (2011). A resource of Cre driver lines for genetic targeting of GABAergic neurons in cerebral cortex. Neuron *71*, 995–1013.

Terburg, D., Scheggia, D., Triana Del Rio, R., Klumpers, F., Ciobanu, A.C., Morgan, B., Montoya, E.R., Bos, P.A., Giobellina, G., van den Burg, E.H., et al. (2018). The basolateral amygdala is essential for rapid escape: A human and rodent study. Cell *175*, 723–735.e16.

Tovote, P., Fadok, J.P., and Lüthi, A. (2015). Neuronal circuits for fear and anxiety. Nat. Rev. Neurosci. *16*, 317–331.

Tovote, P., Esposito, M.S., Botta, P., Chaudun, F., Fadok, J.P., Markovic, M., Wolff, S.B., Ramakrishnan, C., Fenno, L., Deisseroth, K., et al. (2016). Midbrain circuits for defensive behaviour. Nature *534*, 206–212.

Ungless, M.A., and Grace, A.A. (2012). Are you or aren't you? Challenges associated with physiologically identifying dopamine neurons. Trends Neurosci. *35*, 422–430.

van Zessen, R., Phillips, J.L., Budygin, E.A., and Stuber, G.D. (2012). Activation of VTA GABA neurons disrupts reward consumption. Neuron *73*, 1184–1194.

Watabe-Uchida, M., Zhu, L., Ogawa, S.K., Vamanrao, A., and Uchida, N. (2012). Whole-brain mapping of direct inputs to midbrain dopamine neurons. Neuron *74*, 858–873.

Wei, P., Liu, N., Zhang, Z., Liu, X., Tang, Y., He, X., Wu, B., Zhou, Z., Liu, Y., Li, J., et al. (2015). Processing of visually evoked innate fear by a non-canonical thalamic pathway. Nat. Commun. *6*, 6756.

Wickersham, I.R., Lyon, D.C., Barnard, R.J., Mori, T., Finke, S., Conzelmann, K.K., Young, J.A., and Callaway, E.M. (2007). Monosynaptic restriction of transsynaptic tracing from single, genetically targeted neurons. Neuron *53*, 639–647.

Yamaguchi, T., Sheen, W., and Morales, M. (2007). Glutamatergic neurons are present in the rat ventral tegmental area. Eur. J. Neurosci. *25*, 106–118.

Yang, H.B., Yang, J.H., Xi, W., Hao, S.J., Luo, B.Y., He, X.B., Zhu, L.Y., Lou, H.F., Yu, Y.Q., Xu, F.Q., et al. (2016). Corrigendum: Laterodorsal tegmentum interneuron subtypes oppositely regulate olfactory cue-induced innate fear. Nat. Neurosci. *19*, 862.

Ydenberg, R.C., and Dill, L.M. (1986). The Economics of Fleeing from Predators. Adv. Stud. Behav. *16*, 229–249.

Yilmaz, M., and Meister, M. (2013). Rapid innate defensive responses of mice to looming visual stimuli. Curr. Biol. *23*, 2011–2015.

Yu, K., Garcia da Silva, P., Albeanu, D.F., and Li, B. (2016). Central amygdala somatostatin neurons gate passive and active defensive behaviors. J. Neurosci. *36*, 6488–6496.

Zelikowsky, M., Hui, M., Karigo, T., Choe, A., Yang, B., Blanco, M.R., Beadle, K., Gradinaru, V., Deverman, B.E., and Anderson, D.J. (2018). The neuropeptide Tac2 controls a distributed brain state induced by chronic social isolation stress. Cell *173*, 1265–1279.e19.

Zhao, X., Liu, M., and Cang, J. (2014). Visual cortex modulates the magnitude but not the selectivity of looming-evoked responses in the superior colliculus of awake mice. Neuron *84*, 202–213.

## STAR★METHODS

### KEY RESOURCES TABLE

| REAGENT or RESOURCE | SOURCE | IDENTIFIER |
|---|---|---|
| Antibodies | | |
| Rabbit anti-c-Fos | Cell Signaling Technology | Cat#2250; RRID: AB_2247211 |
| DAPI | Thermofisher | Cat#62248 |
| Rabbit anti-dsRED | Clontech | Cat#632496; RRID: AB_10013483 |
| Rabbit anti-CamKII*a* | Abcam | Cat#ab52476; RRID: AB_868641 |
| Rabbit anti-GFP | Abcam | Cat#ab290; RRID: AB_303395 |
| Mouse anti-TH | Millipore | Cat#MAB318; RRID: AB_2201528 |
| Goat anti-rabbit IgG(H+L) alexa fluor@594-conjugated affinipure | Jackson immuno research | Cat#111-585-003; RRID: AB_2338059 |
| Goat anti-rabbit alexa fluor@488-conjugated affinipure fab fragment | Jackson immuno research | Cat#111-547-003; RRID: AB_2338058 |
| Goat anti-mouse IgG(H+L) alexa fluor@594-conjugated affinipure | Jackson immuno research | Cat#115-585-003; RRID: AB_2338871 |
| Goat anti-mouse alexa fluor@488-conjugated affinipure fab fragment | Jackson immuno research | Cat#115-547-003; RRID: AB_2338869 |
| Bacterial and Virus Strains | | |
| AAV2/9-*CaMKIIa*-hChR2(H134R)-mCherry | Liping Wang's Lab at the CAS | N/A |
| AAV2/9-*CaMKIIa*:: eNpHR3.0-mCherry | Liping Wang's Lab at the CAS | N/A |
| AAV2/9-*CaMKIIa*:: mCherry | Liping Wang's Lab at the CAS | N/A |
| AAV2/9-*Ef1*$\alpha$:: DIO-hChR2(H134R)-mCherry | Liping Wang's Lab at the CAS | N/A |
| AAV2/9-*Ef1*$\alpha$:: DIO-eNpHR3.0-mCherry | Liping Wang's Lab at the CAS | N/A |
| AAV2/9-*Ef1*$\alpha$::DIO-mCherry | Liping Wang's Lab at the CAS | N/A |
| AAV2/9-*Ef1*$\alpha$::DIO-GFP | BrainVTA Co., Ltd.,China | N/A |
| AAV2/9-*Ef1*$\alpha$:: DIO-GCaMP6s | BrainVTA Co., Ltd.,China | N/A |
| AAV2/9-*Ef1*$\alpha$:: FDIO-mCherry | BrainVTA Co., Ltd.,China | N/A |
| Retro-AAV2-*Ef1*$\alpha$:: DIO-flp | BrainVTA Co., Ltd.,China | N/A |
| CAV2-Cre | EJ Kremer at the Institute of Molecular Genetics of Montpellier | N/A |
| AAV2/9-*EF1*$\alpha$:: DIO-TVA-GFP | BrainVTA Co., Ltd.,China | N/A |
| AAV2/9-EF1$\alpha$:: DIO-histone-TVA-GFP | BrainVTA Co., Ltd.,China | N/A |
| AAV2/9-*EF1*$\alpha$:: DIO-RV-G | BrainVTA Co., Ltd.,China | N/A |
| RV-EnvA-dG-dsRed | BrainVTA Co., Ltd.,China | N/A |
| Chemicals, Peptides, and Recombinant Proteins | | |
| D-AP5 | Tocris | Cat#79055-68-8 |
| NBQX | Tocris | Cat#118876-58-7 |
| Corticosterone ELISA kit | Abcam | Cat#Ab108821 |
| (+)-Bicuculline | Tocris | Cat# 0130 |
| Experimental Models: Organisms/Strains | | |
| C57BL/6J mice | Guangdong Medical Laboratory Animal Center, Guangzhou, China | N/A |
| TH-Cre mice; 7630403G23RikTg(Th-cre)1Tmd | The Jackson Laboratory | Stock No: 008601 |
| DAT-ires-Cre mice; Slc6a3tm1.1(cre)Bkmn/J | The Jackson Laboratory | Stock No: 006660 |
| GAD2-ires-Cre mice; Gad2tm2(cre)Zjh/J | The Jackson Laboratory | Stock No: 010802 |

(*Continued on next page*)

*Continued*

| REAGENT or RESOURCE | SOURCE | IDENTIFIER |
|---|---|---|
| Software and Algorithms | | |
| ANY-maze video tracking software | Stoelting Co., IL, USA | N/A |
| GraphPad Prism 7.0 | GraphPad Software Inc | https://www.graphpad.com/scientific-software/prism/ |
| MATLAB R2014a | The MathWorks, Inc. | https://ch.mathworks.com/products/matlab |
| pClamp 10 | Axon instruments | https://www.moleculardevices.com/ |
| Anymaze® | Anymaze® | http://www.anymaze.co.uk/ |
| Offline Sorter V4 | Plexon Inc | http://plexon.com/ |
| neuroexplorer V5 | Plexon Inc | http://plexon.com/ |
| ImageJ | NIH | https://imagej.nih.gov/ij/ |
| Image Pro-plus | Media Cybernetics, Inc | https://en.freedownloadmanager.org/Windows-PC/Image-Pro-Plus.html |
| Zen softwares | Zeiss | https://www.zeiss.com/corporate/en_de/global/home.html |
| Adobe Photoshop CC2015 | Adobe Systems Inc | https://www.adobe.com/ |

## CONTACT FOR REAGENT AND RESOURCE SHARING

Further information and requests for resources and reagents should be directed to and will be fulfilled by the Lead Contact, Liping Wang (lp.wang@siat.ac.cn); Fuqiang Xu, (fuqiang.xu@wipm.ac.cn)

## EXPERIMENTAL MODEL AND SUBJECT DETAILS

### Animals

All husbandry and experimental procedures in this study were approved by the Animal Care and Use Committees at the Shenzhen Institute of Advanced Technology (SIAT) or Wuhan Institute of Physics and Mathematics (WIPM), Chinese Academy of Sciences (CAS). Adult (6 to 8 week-old) male C57BL/6J (Guangdong Medical Laboratory Animal Center, Guangzhou, China), TH-Cre (Jax No. 008601) (Savitt et al., 2005), GAD2-ires-Cre (Jax No. 010802) (Taniguchi et al., 2011) and DAT-ires-Cre (Jax No. 006660) (Ekstrand et al., 2007) mice were used in this study. Mice were housed at 22-25°C on a circadian cycle of 12-hour light and 12-hour dark with *ad-libitum* access to food and water.

## METHOD DETAILS

### Viral vector preparation

For optogenetic experiments, we used plasmids for AAV2/9 viruses encoding *CaMKIIa*:: hChR2 (H134R)-mCherry, *CaMKIIa*:: eNpHR3.0-mCherry, *CaMKIIa*:: mCherry, *EF1α*:: DIO-hChR2 (H134R)-mCherry, and *EF1α*:: DIO-eNpHR3.0- mCherry (all gifts from Dr. Karl Deisseroth, Stanford University). Viral vector titers were in the range of 3-6x$10^{12}$ genome copies per ml (gc)/ml. For AAV2/9 viruses encoding *EF1α*:: FDIO-mCherry, *EF1α*:: DIO-GCaMP6s and *EF1α*:: DIO-GFP were all packaged by BrainVTA Co., Ltd., Wuhan. For rabies tracing, Retro-AAV-*Ef1α*::DIO-flp packaged by BrainVTA Co., Ltd. with 1.8 x$10^{13}$ genome copies per ml (gc)/ml., Wuhan with viral vectors AAV2/9-*EF1α*-:: DIO-TVA-GFP, AAV2/9-*EF1α*:: DIO-histone-TVA-GFP, AAV2/9-*EF1α*:: DIO-RV-G, and RV-EnvA-dG-dsRed were all packaged by BrainVTA Co., Ltd., Wuhan. For retrograde tracing, Adeno-associated and rabies viruses were purified and concentrated to titers at approximately 3 × $10^{12}$ v.g /ml and 1 × $10^{9}$ pfu/ml, respectively. The canine adenovirus type-2 encoding Cre recombinase (Kremer et al., 2000) (CAV2-Cre, 4 × $10^{12}$ v.g/ml) was provided by EJ Kremer at the Institute of Molecular Genetics of Montpellier.

### Virus injection

Animals were anesthetized with pentobarbital (i.p., 80 mg/kg), and then placed in a stereotaxic apparatus (RWD, China). During surgery and virus injections, animals were kept anesthetized with isoflurane (1%). The skull above targeted areas was thinned with a dental drill and carefully removed. Injections were conducted with a 10 μL syringe connected to a 33-Ga needle (Neuros; Hamilton, Reno, USA), using a microsyringe pump (UMP3/Micro4, USA). Experiments were performed at least 5-8 weeks after virus injection. Coordinates for virus injection of the SC (total volume of 300 nl-400 nl) were: anterior posterior (AP), −3.80 mm; medial lateral (ML), ± 0.80 mm; dorsoventral (DV), −1.8 mm. VTA (total volume of 120 nl) coordinates were: AP −3.20 mm, ML ± 0.25 mm, and DV −4.4 mm. Amygdala (total volume of 80 nl) coordinates were: AP, −1.5 mm; ML, ± 2.95 mm; DV, −4.75 mm. Viruses were delivered unilaterally for ChR2 and bilaterally for eNpHR3.0, GCaMP6s and GFP.

### *Trans*-synaptic tracer labeling

All animal procedures were performed in Biosafety level 2 (BSL2) animal facilities. To determine whether the SC-VTA pathway was innervated by GABAergic neurons in the VTA, GAD2-Cre mice (20-25 g) were used for trans-mono-synaptic tracing based on the modified rabies virus. A mixture of AAV2/9-*EF1α*:: DIO-TVA-GFP and AAV2/9-*EF1α*:: DIO-RV-G (1:1, total volume of 150 nl) was injected into the VTA region using the following coordinates: AP, −3.20 mm; ML, −0.25 mm; DV, −4.40 mm. Three weeks later, 200 nL of EnvA-pseudotyped rabies virus (EnvA-RV-dG-DsRed) was injected into the VTA using the previously defined coordinates.

To determine whether the SC-VTA-CeA pathway was innervated by GABAergic neurons in the VTA, we modified the mono-synaptic rabies tracing strategy. On the first day, we injected a mixture of 120 nL AAV2/9-*EF1α*:: DIO-histone-TVA-GFP and AAV2/9-*EF1α*:: DIO-RV-G (1:1) into the VTA of GAD2-ires-Cre mice. Six weeks later, when the accumulated TVA of GABAergic VTA neurons was transported to axon terminals in the CeA, we injected 200 nL of EnvA-RV-dG-dsRed into the CeA (AP, −1.5 mm; ML, 2.95 mm; DV, −4.75 mm) of these mice. Thus, we specifically infected CeA-projecting GABAergic VTA neurons and traced their inputs. Mice were sacrificed one week after RV injection.

### Implantation of optical fiber(s) and cannulas

To optically stimulate terminals, a 200 μm optic fiber (NA: 0.37; NEWDOON, Hangzhou) was unilaterally implanted into the SC (AP, −3.8 mm; ML, −0.6 mm; DV, −1.4 mm) and VTA (AP, −3.20 mm; ML, −0.25 mm; DV, −3.8 mm). For the inhibition of neuron soma or projections, optic fibers were bilaterally implanted into the VTA (AP, −3.20 mm; ML, ± 1.50 mm; DV, −4.0 mm) at a 15° angle from the vertical axis. For fiber photometry, the optic fiber was implanted into the VTA of GAD2-Cre mice (AP, −3.20 mm; ML, −1.5 mm; DV, −4.4 mm) at a 15° angle. For pharmacological experiments, drug cannulas were bilaterally implanted into the VTA (AP, −3.20 mm; ML, ± 0.35 mm; DV, −3.8 mm) and CeA (AP, −1.3 mm; ML, ± 2.95 mm; DV, −4.2 mm). Mice had at least 1-2 weeks to recover after surgery.

## PATCH-CLAMP ELECTROPHYSIOLOGY

We use standard procedures to prepare coronal slices (300 μm) from 14-16 weeks old GAD2-ires-Cre and TH-Cre mice, which had received virus injections six weeks earlier. Recordings in VTA were made on visually identified neurons expressing EYFP. Coronal sections were cut with a vibratome (Leica) into a chilled slicing solution containing the following (in mM): 110 Choline Chloride, 2.5 KCl, 1.3 1.3 $NaH_2PO_4$, 25 $NaHCO_3$, 1.3 Na-Ascorbate, 0.6 Na-Pyruvate, 0.5 $CaCl_2$, 7 $MgCl_2$). Then, slices were incubated at 32 °C for 30 min in artificial cerebrospinal fluid (ACSF) which contained (in mM): 125 NaCl, 2.5 KCl, 1.3 $NaH_2PO_4$, 25 $NaHCO_3$, 1.3 Na-Ascorbate, 0.6 Na-Pyruvate, 10 Glucose, 2 $CaCl_2$, 1.3 $MgCl_2$ (pH 7.35 when saturated with 95% $O_2$/ 5% $CO_2$), and allowed to equilibrate to room temperature for > 30 min. The osmolarity of all solutions was maintained at 280–300 mOsm.

Evoked EPSCs were induced using 1 s blue light (5 ms pulse, 20 Hz) stimulation of VTA terminals of CaMKIIα positive neurons expressing ChR2 from SC soma projecting to VTA. Recordings were performed on GAD2+ neurons (EYFP positive), TH+ (EYFP positive) or TH- (EYFP negative) with pipettes filled with the following (in mM): (105 Potassium gluconate, 30 KCl, 10 HEPES, 10 phosphocreatine, 0.3 EGTA, 5 QX314, 4 Mg-GTP, 0.3 Na-ATP, pH 7.35. To identify the eEPSCs glutamatergic nature, ionotropic glutamate receptor antagonists, d-2-amino-5-phosphonovalerate (AP-5; 25 μM) and 2, 3-dihydroxy-6-nitro-7-sulfamoyl-benzoquinoxaline-2, 3-dione (NBQX; 20 μM) were added at the end of recordings.

Evoked IPSCs were elicited using 1 s blue light (5 ms pulse, 60 Hz) stimulation of CeA axon terminals of GABAergic neurons expressing ChR2 VTA axons projecting to CeA. Recordings were performed on CeA neurons with pipettes filled with the following (in mM): 130 mM cesium gluconate, 7 mM CsCl, 10 mM HEPES, 2 mM $MgCl_2$, 4 mM Mg-ATP, 0.3 mM Tris-GTP, and 8 mM QX314, pH 7.25. To rule out glutamatergic inputs, ionotropic glutamate receptor antagonists, AP-5 (25 μM) and NBQX (20 μM) were added to the artificial cerebrospinal fluid. To identify the eIPSCs GABAergic nature, GABA-A receptors with bicuculline (25 μM) was added at the end of recordings.

Several criteria had to be met for successful inclusion of recording data: 1) The amplitude of eIPSCs or eEPSCs was higher than 10 pA; 2) latency was less than 10 ms for at least 60% of the trials. 3) Whole-cell patch-clamp recordings were discarded if the access resistance exceeded 10 MΩ and changed more than 25% during the recordings.

Pipettes were formed by a micropipette puller (Sutter P-2000) with a resistance of 3−5 MΩ. During whole-cell patch recording, we viewed individual cells with an upright fixed-stage microscope (FN-S2N; Nikon, Japan) equipped with a water immersion objective (40 ×, 0.8 numerical aperture), IR-filtered light, differential interference contrast optics, and a Coolsnap HQ CCD camera (Photomatrics, Britannia). All recordings were conducted with a MultiClamp700B amplifier (Molecular Devices). Analog signals were low-pass filtered at 2 kHz, digitized at 20 kHz using Digidata 1440A, and recorded using pClamp 10 software (Molecular Devices).

Data are presented as means ± standard error of the mean (SEM). Statistical significance was determined using a two-tailed Student's t test or a two-way analysis of variance (ANOVA), with a significance level of $p < 0.05$.

### Histology, immunohistochemistry, and microscopy

Mice received an overdose of chloral hydrate (10% W/V, 300 mg/kg body weight, i.p.) and were then transcardially perfused with cold phosphate-buffered saline (PBS), followed by ice-cold 4% paraformaldehyde (PFA; Sigma) in PBS. Brains were removed and submerged in 4% PFA at 4°C overnight to post-fix, and then transferred to 30% sucrose to equilibrate. Coronal brains sections (40 μm)

were obtained on a cryostat microtome (Lecia CM1950, Germany). Freely floating sections were washed with PBS, blocking solution (0.3% Triton X-100 and 10% normal goat serum, NGS in PBS, 1 h at room temperature). Sections were then incubated in primary antiserum (rabbit anti-c-Fos, 1:300, Cell Signaling; Rabbit anti-CaMKII$\alpha$, 1:250, Abcam; 1:1000, Abcam; rabbit anti-TH, 1:500, Abcam; mouse anti-TH, 1:500, Millipore; rabbit anti-dsRed, 1:1000, Clontech;rabbit anti-GFP, 1:500, Abcam) diluted in PBS with 3% NGS and 0.1% Triton X-100 overnight. The secondary antibodies used were Alexa fluor 488, 594, or 405 goat anti-mouse IgG and Alexa fluor 488, 594, or 405 goat anti-rabbit (all 1:200, Jackson) at room temperature for 1 h. Sections were mounted and covered slipped with anti-fade reagent with DAPI (ProLong Gold Antifade Reagent with DAPI, life technologies) or signal enhancer (Image-iT FX Signal Enhancer, Invitrogen). Sections were then photographed and analyzed with a Leica TCS SP5 laser scanning confocal microscope and ImageJ, Image Pro-plus, and Photoshop software.

For the retrograde tracing (retro-AAV) plus looming-evoked c-Fos staining, rabies mon-synaptic tracing plus looming-evoked c-Fos staining and only looming-evoked c-Fos staining experiments, mice were sacrificed 1.5 hr post looming stimulus and brains then subjected to c-Fos staining. The imagines were taken and then overlaid with The Mouse Brain in Stereotaxic Coordinates to locate the VTA (with coordinates from bregma: $-2.9\sim3.8$ mm). Then the c-Fos staining was manually counted by an individual experimenter blind to the experiment groups.

### Plasma corticosterone measurement

Animals were euthanized by rapid decapitation and trunk blood was collected into heparinized tubes 10 min after optic stimulation (50 pulses, 20 Hz blue light, 5 ms pulse duration). After centrifugation of the blood at 3000 rpm for 20 min at 4°C, the serum was stored at −80°C until assay. Plasma corticosterone level was measured using a commercially available ELISA kit (Abcam).

### Electrocardiogram recording

Heart rate (HR) recordings were measured using the MouseOX® Plus non-invasive pulse oximeter (STARR Life Sciences, Oakmont, PA). The neck collar and system were set up according to manufacturer instructions. After a baseline recording of 5 min, 5 photostimulation trials were applied (50 pulses, 20 Hz, 3 min inter-spike interval [ISI]). Data were extracted using WINDAQ software (© DATAQ). HR data was then analyzed with custom-written MATLAB scripts. HR time courses were obtained by averaging data from each trial around the time of stimulation. Error bars represent mean ± SEM.

### Looming test

The looming test was performed in a 40 × 40 × 30 cm closed Plexiglas box with a shelter nest in the corner. For upper field LS, an LCD monitor was placed on the ceiling to present multiple looming stimulus. For upper visual field LS, an LCD monitor was placed on the ceiling to present multiple looming stimuli, which was a black disc expanding from a visual angle of 2° to 20° in 0.3 s, i.e., expanding speed of 60°/s. The expanding disc stimulus was repeated for 15 times in quick succession (totally 4.5 s). This together with a 0.066 s pause between each repeat, the total upper visual field LS last 5.5 s.

Lower field LS (same stimulus as above but presented to the lower field), upper field white LS (a disc of reversed contrast (white on gray) presented to the upper field) and front field LS (the same black stimulus except presented to the front field) were used as control visual stimulus.

Behavior was recorded using an HD digital camera (Sony, Shanghai, China). Animals were handled and habituated for 10-15 min to the looming box one day before testing. During the looming test session, mice were first allowed to freely explore the looming box for 3-5 min. For optogenetic, c-Fos and pharmacological experiments plus looming experiment, we performed 2 trials of looming stimuli while only the first defensive behavior output was analyzed; for calcium signal experiment, total 5 trials of looming stimuli were presented and analyzed. No observable adaptation was observed in all our experiments.

The optogenetic inhibition/stimulation and the looming stimulus were coupled by ARBITRARY/FUNCTION GENERATOR (AFG3022B, Tektronix, USA). We manually the triggered stimulation when the mice were at the far-end of the open-field as to the nest position, within in a body-length distance from the wall.

### Optogenetic manipulation

Animals were handled and habituated for 10-15 min to the looming box one day before testing. During the Looming test session, mice were first allowed to freely explore the looming box for 3-5 min, then received the optogenetic manipulation or looming stimulus.

For optogenetic NpHR inhibition plus looming experiments, mice received bilateral 593 nm yellow light laser (Aurora-220-589, NEWDOON, Hangzhou) with 5-8 mW (for soma stimulation) or 15-20 mW (for terminals stimulation) light power at the fiber tips. Light stimulation was delivered 1 s before onset of the looming stimulus and continued until the looming was turned off. For optogenetic NpHR inhibition of VTA DAT neurons without looming, mice received 2.5 s bilateral continuous 593 nm yellow light stimulation. Light was presented two times at about 3 min intervals via a manual trigger.

For optogenetic activation experiments, mice were placed into the same looming box and received a 2.5 s 473-nm blue laser (Aurora-220-473, NEWDOON, Hangzhou) (50 pulses, 20 Hz, 5 ms pulse duration) with 15-20 mW (terminal) or 5-8 mW (soma) light power at the fiber tips. No looming was presented for these experiments. Light stimulation was delivered to the SC and VTA somas, as well as the SC-VTA terminals. For the activation of $VTA^{GABA+}$ neurons experiments, the GAD2-Cre mice received 2.5 s or 20 s blue light (60 Hz, 5 ms pulse duration, 5-8 mW) stimulation in the VTA; For the activation of $VTA^{DA+}$ neurons experiments, the DAT-Cre mice

received 2.5 s blue light (10 Hz, 5 ms pulse duration, 5-8 mW) stimulation in the VTA; For optogenetic ChR2 excitation plus looming experiments, mice received bilateral 10 Hz, 473 nm blue light laser and light stimulation was delivered 1 s before onset of the looming stimulus and continued until the looming was turned off. There no other experimental details were changed. Light was presented two times at about 3 min intervals via a manual trigger.

All light stimulation was manually presented by the experimenter when the mice were at the far-end of the open-field as to the nest position, within in a body-length distance from the wall.

For all our lost-of function experiments (optical inhibition by NpHR), the inhibition was all bilateral. For all our gain-of function experiments (optical activation of ChR2), the activation was all unilateral.

## PHARMACOLOGICAL ANTAGONISM

C57BL/6J mice were used for pharmacological experiments. For the CeA experiment, 150 nL $GABA_A$ antagonist (0.005 μg Bicuculline) was bilaterally injected into the CeA (AP, −1.5 mm; ML, ± 2.95 mm; DV, −4.6 mm). For optogenetic ChR2 activation of VTA GAD2+ neurons plus looming experiments, mice received unilateral 60 Hz blue light with 5-8 mW light power at the fiber tips. Antagonism (bicuculline) was delivered 30 min before onset of the 473 nm blue light. After 24 hr, mice received 60 Hz blue light stimulation again without plus antagonism. Mice were given 1-2 weeks to recover after surgery. Saline (control) and antagonists were infused into the targets 30 min before a looming test to assess the antagonistic effect of the antagonism receptors.

### Behavioral analysis

Behavioral data were analyzed with Anymaze software (Stoelting Co.). Speed data was first extracted using Anymaze software and then analyzed using MATLAB. Individual time courses were represented setting T-0 ms as the time of stimulation. The following measures were obtained as indices of looming-evoked or light-evoked defensive behaviors: (1) latency to return nest: the time from looming stimulus or photostimulation presentation to time when the mouse escaped/entered the nest; (2) time spent in nest (% of 1 min bin): time spent in the nest following looming stimulus or photostimulation; (3) speed. The mice were allowed to move freely in the open field with a nest paradigm before looming stimulus or light stimulation. The mice were moving freely when looming stimulus or light stimulation began. Here, ''baseline'' was defined as the period 50 s before onset of the looming or light stimulation. The average speed during the baseline period was set as 100%. We have presented all speeds in relative percentage form compared with baseline average speed. For the speed bar graphs: post-stimulation speed was averaged over a 0.5 s-long time window centered around the time of maximum speed, detected from the time of stimulation to 10 s after.

For all mice used, after our data were collected, virus expression and cannula or fiber placements were confirmed by histological staining. Virus expression, behavioral tests and behavior analyses were performed by different people. Decisions to discarded data on any given day was done blind to the behavioral experiments.

### *In vivo* electrophysiology

The optrode was an optic fiber (0.37 NA, 200 μm) attached around eight stereotrodes, which consisted of insulated nichrome wires (OD = 17 μm; CFW, California, USA). The tips of the stereotrode were electro-plated with platinum with platinum (chloroplatinic acid solution) until the impedance reached approximately 0.5 MΩ and was 0.3 mm longer than the tips of fiber. Data were collected by OmniPlex D Neural Data Acquisition System (Plexon, Dallas, USA). Mice were anesthetized with urethane (10% W/V, 1.9 g/kg body weight, i.p.) and positioned in the stereotaxic apparatus. The optrode was placed into the VTA (AP, −3.20 mm; ML, −0.3 mm; DV, −4.1∼4.7 mm). If the detected signal in the VTA was stable, a 473 nm laser (20 Hz with 5 ms width pulses) was delivered to excite CaMKIIα+ projections from the SC. Baseline was recorded in the VTA for 2-3 min, and a 2.5 s optic stimulation was delivered at 1 min intervals. At the end of the experiment, electrolytic lesions were performed (0.1 mA DC, 20 s) to label the recording side.

### Data analysis

Recorded spikes were detected and sorted by using Plexon Offline Sorter software (Plexon, Inc., Dallas, TX, USA), then analyzed in Neuroexplorer (Nex Technologies, Madison, AL, USA) and MATLAB (MathWorks, Natick, MA, USA). Putative dopamine neurons were classified by agglomerative clusters from linkages based on the following electrophysiological criteria (Tan et al., 2012): 1) low baseline firing rate (< 10 Hz); 2) inter-spike interval (ISI) > 4 ms within a ≥ 99.8% confidence level; 3) half action potential (AP) widths broader ≥ 0.8 ms. In contrast, if neurons did not meet these criteria, they were classified as non-putative DA neurons.

VTA neurons were recorded for around 3 min to establish the discharge properties and basal firing rate of VTA neurons before optical stimulation. The baseline firing rate was calculated using the mean and standard deviation (SD) of firing rate values for every 0.5 s bin 2.5 s preceding optical stimulation. To determine the excitatory and inhibitory response related to photostimulation, we used peristimulus time histograms (PSTHs) to analyze firing pattern (Tan et al., 2012). 1) Excitation: the PSTH 20 ms (0.5 ms per bin) following the light pulses was calculated. The neuronal responses were defined as the 3 consecutive bins after the onset of light stimulation triggered the PSTH that exceeded the 2 SDs of baseline value. 2) Inhibition: the PSTH in 10 s (0.2 s per bin) following the light pulses was calculated. Neuronal inhibition was defined as the 5 consecutive bins after onset of light stimulation triggered the PSTH that dropped to at least 35% below baseline value. The magnitude of the normalized firing rate was calculated according to

the following equation: Magnitude = (counts in response period)- (mean counts per bin in baseline) x (number of bins during the response period).

### Fiber Photometry

The fiber photometry system (ThinkerTech, Nanjing) consisted of a 480 nm excitation light from a LEDs (CREE XPE), reflected off a dichroic mirror with a 435–488 nm reflection band and a 502–730 nm transmission band (Edmund, Inc.), and coupled into a 200 μm 0.37 NA optical fiber (Thorlabs, Inc.) by an objective lens. The laser intensity at the fiber tip was about 20 μW. GCaMP6s fluorescence was collected using the same objective, transmitted by the dichroic mirror filtered through a green fluorescence protein (GFP) band-pass emission filter (Thorlabs, Inc. Filter 525/39), and detected by the sensor of an CMOS camera (Thorlabs, Inc. DCC3240M).

A Labview program was developed to control the CMOS camera which recorded calcium signals at 50 Hz. The behavioral event signal was recorded by a DAQ card (NI, usb-6001) at 1000 Hz using the same program.

## DATA ANALYSIS

All the raw data were smoothed with a moving average filter (5-point span) and then segmented and aligned according to the onset of looming stimulus within individual trials or bouts. The fluorescence change ($\Delta F/F$) values were calculated as $(F-F_0)/F_0$, where $F_0$ is the baseline fluorescence signals averaged over a 2 s-long control time window (typically set 1 s) prior to a trigger event.

To compare activity between different conditions, bar graphs were computed by averaging data along a 0.5 s time window centered around the time of the activity pic. Time courses were made by averaging individual trials aligned to the time of stimulation. A multivariate permutation (1000 permutations, $\alpha$ level of 0.05) test was used to account for data significance level on time courses, and a threshold indicating statistically-significant increase from the baseline was applied ($p < 0.005$). Areas surrounding the time courses and error bars represents mean ± SEM.

## QUANTIFICATION AND STATISTICAL ANALYSIS

The number of biological replicates in each group was 3-9 mice per group for anatomy, 4-8 mice for *in vitro* and *in vivo* physiology, 5-7 mice per group for fiber photometry, and 5-16 mice per group for behavior. These numbers were based on previously published study (Wei et al., 2015; Tovote et al., 2016). Data distribution was assumed to be normal, but this was not formally tested. All statistics were performed in Graph Pad Prism (GraphPad Software, Inc.), unless otherwise indicated. Paired student test, unpaired student test, one-way ANOVA and two-way ANOVA were used where appropriate. Bonferroni post hoc comparisons was conducted to detect significant main effects or interactions. In all statistical measures a P value $< 0.05$ was considered statistically significant. Post hoc significance values were set as $^*p < 0.05$, $^{**}p < 0.01$, $^{***}p < 0.001$ and $^{****}p < 0.0001$; all statistical tests used are indicated in the figure legends.